Bonding and structures in silicon clusters: A valence-bond interpretation

Charles H. Patterson*
Department of Physics, University of Pennsylvania, Philadelphia, Pennsylvania 19104-6396

Richard P. Messmer
General Electric Corporate Research and Development, Schenectady, New York, 12301
and Department of Physics, University of Pennsylvania, Philadelphia, Pennsylvania 19104-6396
(Received 25 January 1990; revised manuscript received 7 May 1990)

Electronic-structure calculations using the *ab initio* generalized-valence-bond approach have been used to investigate the structure and bonding of silicon clusters Si_3–Si_{10}. While several previous studies of the structures of these clusters have been presented, this is the first to provide an in-depth analysis of the bonding. The importance of including electronic correlation effects self-consistently in determining the cluster structures is emphasized. New geometrical structures are found for Si_8 and Si_{10} that have nearly identical energies to previously proposed structures. In addition, for Si_6 we find the relative stabilities of two structures to be reversed from previous work, leading to a different ground state. It is found that these clusters exhibit bonding characteristics typical of both metals (charge density in interstitial regions) and covalent semiconductors (charge density between pairs of atoms). The insight gained regarding the bonding in the small clusters is used to predict the structures for larger "magic-number" silicon clusters containing 21, 25, 33, 39, and 45 atoms, whose positive ions are found experimentally to have significantly lower reactivities than the ions containing other numbers of atoms. These proposed cluster structures are based on 17-atom bulklike cores whose surfaces resemble those found in reconstructed silicon surfaces. The relationship of the bonding in the small clusters to the bonding at surfaces is also considered. The analogies are quite striking and strongly suggest that local-bonding considerations may be a critical component in understanding the structures and properties in both situations.

I. INTRODUCTION

In the past four years a considerable amount of experimental and theoretical effort has been expended in the study of semiconductor and metal clusters. Advances in experimental methods have made possible the formation of size- and charge-selected clusters—allowing studies by the techniques mentioned below. Theoretical studies of silicon clusters have focused on the equilibrium geometries of clusters in the size range 2–20 atoms, but the complexity and variety of bonding modes that exist in these clusters has not been recognized.

Experimental techniques that have been applied to silicon clusters include photodetachment of negative ions,[1] two-photon-ionization studies,[2] studies of their chemical reactivities,[3–7] collision-induced dissociation,[8] and photofragmentation[9–12] of positive and negative ions. They have revealed similar properties for covalently bonded silicon and germanium clusters that are in sharp contrast to those of metal clusters[13] or GaAs clusters.[10] For example, photodetachment spectra[1] (negative-ion ultraviolet photoelectron spectra) have shown that neutral silicon and germanium clusters have similar electronic spectra. Clusters and cluster ions in the beam are expected to be in their electronic and vibrational ground states[1] because of the rapid expansion of the vapor into the vacuum. Photodetachment spectra may therefore be interpreted as resulting from ionization of the ground-state anion, which leaves the neutral cluster in either its ground state or one of its excited states. In the size range 3–12 atoms, similarities in the photodetachment spectra[1] of silicon and germanium imply that, for each cluster size, they have *structures* of the same symmetry. Two-photon-ionization studies have revealed long-lived excited states, a characteristic of semiconductors, for neutral Si_{10} and Ge_{10} clusters[2] but much shorter-lived excited states for clusters of metal atoms.[13] The lifetime[2] of a 1.5-eV excitation in Si_{10} is 3.4 ns; in contrast, the lifetime of a 1-eV excitation in Cu_3 is of the order of picoseconds.[13] Chemical reactivity studies of silicon clusters in the size range 7–65 atoms[5] present the best currently available experimental evidence for the structures of larger silicon clusters. The data show "a series of dramatic oscillations in reactivity" for clusters in the size range just mentioned. Chemically less reactive clusters had fewer than 14 atoms or had 21, 25, 33, 39, or 45 atoms. Such clusters had reactivities up to 2 orders of magnitude less than clusters that did not possess such a "magic number" of atoms. This oscillation in chemical reactivity as a function of size is believed to reflect completion of stable units in the clusters with 20 or more atoms and this may be a clue to their structures. In experiments producing photofragmentation or collision-induced dissociation, silicon, and germanium cluster cations with ~15–60 atoms apparently "explode" to yield positive and neutral fragments in the size range 6–11 atoms.[8,10] This is in contrast to metal clusters[13] and GaAs clusters,[10] which photofragment in a sequential fashion, losing one atom at a

time. Fragments of semiconductor clusters with 6, 7, or 10 atoms apparently have a greater stability because of their abundance in these experiments.[8,10]

Ab initio electronic-structure calculations have been used to predict lowest-energy structures for Si clusters in the size range 2–14 atoms;[15–24] larger clusters have been studied using semiempirical techniques but these are not considered here. What has emerged from the *ab initio* work is that for clusters with more than 5 atoms there are several structures with energies close to that of the lowest-energy geometry. Experimental evidence for structural changes in clusters with 10 or more atoms at a finite temperature has recently been presented.[14] As discussed below, it is extremely important to include electron-correlation effects in attempting to determine the lowest-energy structures of a particular size cluster and whether such a cluster is likely to be able to thermally convert from one structure to another.

The most extensive work so far has been carried out by Raghavachari and co-workers.[15–18] They report geometry optimizations of silicon clusters with 3–10 atoms with several different symmetries for each cluster using the (uncorrelated) Hartree-Fock (HF) wave function. Total energies that include electron correlation effects were then evaluated at the HF minima using a fourth order Møller-Plesset perturbation scheme (MP4). Their calculations have also been used to interpret fragmentation of cluster cations[19] in the size range 2–20 atoms.

Four other *ab initio* calculations on the silicon-cluster structures have also been reported recently. Tomanek and Schlüter[20] have optimized geometries of clusters in the size range 2–14 atoms using a local-density-functional (LDF) method; Pacchioni and Koutecky[21] and Balasubramanian[22,23] have performed configuration-interaction (CI) calculations and have optimized geometries for clusters with 3–7 atoms and 3 or 4 atoms, respectively; Ballone *et al.*[24] have used simulated annealing techniques to find minimum-energy structures for silicon clusters with 7–10 atoms. All of these calculations are largely in agreement as to the equilibrium structures for these clusters.

Because of the length of the present paper, which attempts to summarize in one place all the relevant information of our silicon-cluster studies, it may be useful to provide the reader with a brief outline of the content of the paper and introduce some of the key concepts to be described at length below. This is the purpose of the remainder of this introductory section.

The geometries of the clusters were optimized using a generalized-valence-bond (GVB) wave function or for the larger clusters using a HF wave function with a GVB calculation performed at the HF equilibrium geometry. The particular form of the GVB wave function used in this study is described in Sec. II. There are two reasons for choosing such a valence-bond wave function: first, the GVB wave function has the advantage that the single-particle orbitals are unique and may be directly used to interpret the nature of the bonding (e.g., a covalent bond in the GVB wave function is represented by two overlapping orbitals localized on two different atoms with singlet-paired spins); second, the GVB wave function incorporates important intrapair-correlation effects neglected by the HF wave function. As described below this can be very important in determining the relative energies between structures of different bonding types.

In Sec. III the results of the computations on small clusters are described. For a number of the cluster structures, a key feature of the valence-bond description of the electronic structure is that each atom is surrounded by a tetrahedrally oriented set of orbitals. We refer to these as tetrahedral-bond-network (TBN) clusters. In the valence-bond description, pairs of occupied orbitals are singlet spin coupled into *electron pairs,* and these pairs are spatially separated from one another due to the Pauli exclusion principle. This is illustrated schematically in Fig. 1 with a series of TBN clusters with 5–8 atoms. There are typically three types of electron pairs in these clusters that are labeled in Fig. 1(a): (i) bent bonds (BB); (ii) long bonds (LB), and (iii) lone pairs (LP). In Fig. 1(a), for example, there are six symmetry equivalent *bent bonds* that arise from the overlap of two orbitals, one from each of two atoms, that are not directed along the internuclear axis. Only two of these are shown explicitly in Fig. 1(a), while the other four are denoted by a heavy black line connecting the appropriate atoms. The *long bonds* occur when two colinear tetrahedral orbitals on different atoms are pointing away from each other but

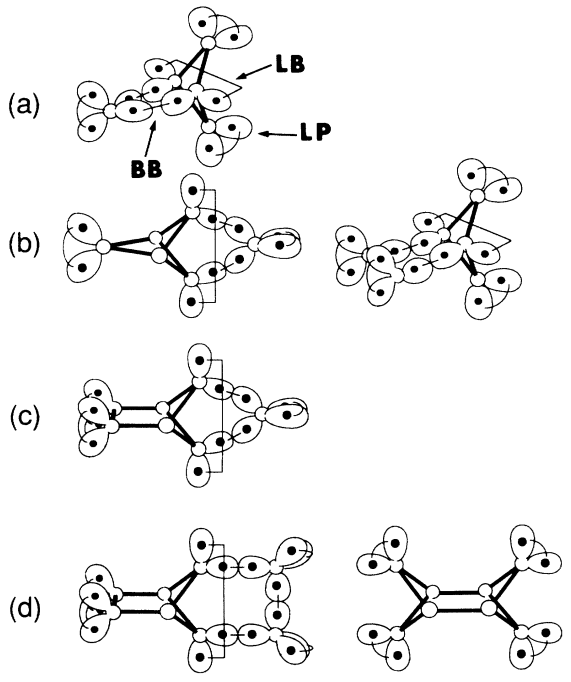

FIG. 1. TBN clusters for (a) Si_5, (b) Si_6, (c) Si_7, and (d) Si_8. Bent-bond (BB), long-bond (LB), and lone-pair (LP) electron pairs are indicated for Si_5. The remaining clusters contain only these kinds of electron pairs and singlet pairing of orbitals is indicated by thin lines. Some bent bonds are indicated by thick solid lines and some long bonds are indicated by thick shaded lines to improve clarity of the diagram.

nonetheless overlap enough to form a bond. When two orbitals on a given atom are not singlet coupled to orbitals on other atoms, they become singlet coupled into angularly correlated *lone pairs* (triplet coupling of these pairs results in a wave function with a higher total energy). There are therefore *no remaining unpaired dangling orbitals* in these clusters and they have singlet ground states. It is important to stress that the simple picture given here in terms of tetrahedral orbitals is closely reproduced as regards orientation and spin pairings by the actual computed GVB orbitals described in detail below. Furthermore, none of the atoms in the TBN silicon clusters possesses the classic "octet" of electrons—instead, most atoms are surrounded by three electron pairs.

Another bonding type found in the calculations of silicon clusters and described in Sec. III is referred to as a polyhedral bonding network (PBN). This class of cluster is characterized by interstitial pairs of electrons localized in triangular faces or tetrahedral interstices of the atomic framework. Analysis of such interstitial orbitals in terms of atom-centered orbitals, leads one to conclude that some atoms have more than four orbitals and some fewer—clearly different than the TBN class. The computational results for Si_6, Si_7, and Si_{10} give the most stable geometries as PBN structures. The Si_{10} cluster consists of a tetracapped octahedron[18,20] with capping atoms in a tetrahedral configuration. A schematic of the structure and the orbital picture derived from the GVB calculations are given in Fig. 2(a). Note that the interstitial pairs localize where three tetrahedral orbitals on separate atoms in the octahedron overlap, as in the triangular face formed by atoms numbered 5, 7, and 10. It is interesting to note that pairs of electrons shared among three nuclei are a common and well-established feature of bonding theories[25] for boron hydrides and that they too adopt polyhedral structures that enable the available electron pairs to be shared by a greater number of boron atoms than if electron pairs were exclusively in two-center–two-electron bonds.

The last type of bond found in the silicon-cluster calculations is the *dative* bond. Dative bonds are formed when a singlet-coupled electron pair localized on one atom is shared with other atoms. When a singe atom is bonded in this way to an otherwise stable (e.g., TBN) cluster, one has an example of a *three-center* dative bond, which is schematically illustrated in Fig. 2(b). Thus an electron pair, which would have been "nonbonding" were it a lone pair, contributes to the stability of the cluster by forming a bond. Dative bonds and interstitial pairs are a means of increasing the number of bonding pairs and the effectiveness with which they are shared, while decreasing the number of nonbonding lone pairs (as compared to TBN clusters).

On the basis of the calculations described in Sec. III and the insight gained from them, Sec. IV provides a discussion of the larger silicon clusters and makes predictions for the "magic-number" structures for clusters with 20–50 atoms. The relationship of the bonding in the small clusters to that in *larger clusters* and the *bulk* is of considerable importance and interest. It is germane to

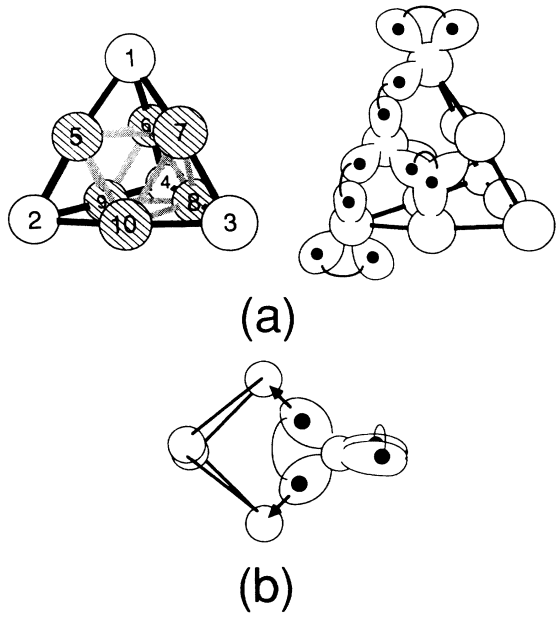

FIG. 2. (a) Geometrical structure and schematic GVB orbital diagrams for T_d Si_{10}. In the structure diagram on the left the central octahedron of atoms is outlined by shaded lines, while the tetrahedral capping atoms are joined to it by solid lines. At the top of the diagram on the right, a capping atom (atom 1 at left) is shown with an angularly correlated lone pair and three bonds to octahedral atoms (one is shown with singlet paired orbitals and the other two are shown with solid lines). In the right diagram the schematic orbitals on one atom (atom 5 at left) of the central octahedron are shown explicitly; those atoms have four tetrahedral orbitals, two are used to form bonds to capping atoms and two form parts of interstitial pairs in different faces of the cluster. An interstitial bond pair (in the triangular face formed by atoms 5, 7, and 10 in the left diagram) is shown at the right. These are all the unique electron pairs in the cluster. (b) Schematic representation of three-center dative bonds.

the development of many-body interatomic force fields for silicon[26–33] that are being applied in *both* bonding environments. There has been speculation that the smaller clusters are metalliclike and the larger clusters are semiconductorlike. Estimates for the cluster size, at which the transition between the two kinds of structures takes place, vary from around 50 atoms[30(b)] to several hundred.[20(b)] By contrast, we argue that clusters with more than twenty atoms have 17-atom bulklike cores with surface structures resembling those found in reconstructions of bulk silicon surfaces and that the smaller clusters exhibit bonding characteristics that are *both* semiconductorlike and metalliclike.

In Sec. V we provide a general discussion of the observed relationships between the structures, bonding, and electron distributions in TBN and PBN clusters on the one hand and the corresponding features in bulk silicon phases and surfaces on the other. Finally, in Sec. VI a brief summary of the main conclusions is provided.

II. THEORETICAL BACKGROUND

A general N-electron wave function may be expressed as a resonating valence-bond (RVB) expansion[34] given by

$$\Psi_{\mathrm{RVB}}=\sum_r c_r \mathcal{A}\left[\prod_i (\varphi_{ir})\Theta_r\right] \tag{1}$$

where $\mathcal{A}$ is the antisymmetrization operator, r is the index over resonance structures, c_r is the coefficient for the rth resonance structure, φ_{ir} is the ith single-particle orbital of the rth resonance structure, and Θ_r is the spin function for the rth resonance structure. When the wave function consists of a single valence-bond (VB) structure and the optimal forms of the single-particle functions and the spin coupling are determined variationally, this is referred to as a GVB wave function. The GVB wave function is the most general single-particle wave function for an electronic system and consists of an antisymmetrized product of (overlapping) spatial orbitals, one for each electron, and a spin function Θ, which is a sum of spin eigenfunctions (i.e., spin functions that are simultaneous eigenfunctions of the S^2 and S_z operators).

The first approximation usually applied, is to restrict the complete spin function to a single spin eigenfunction, θ_{PP}, which is the dominant term in Θ. This is referred to as the *perfect pairing* (PP) approximation[35] and derives its name from the fact that it represents a singlet pairing of electrons in two orbitals. This spin eigenfunction therefore has the form

$$\theta_{\mathrm{PP}}=(\alpha\beta-\beta\alpha)(\alpha\beta-\beta\alpha)(\alpha\beta-\beta\alpha)\cdots . \tag{2}$$

Conceptually one may now legitimately draw "bonds" between orbitals coupled in this way. Furthermore, orbitals of GVB wave functions generally localize into bond *pairs* and lone *pairs* and thus a link is readily established between familiar chemical bonding concepts and the actual theoretical calculation. It is convenient to label orbitals singlet coupled into the ith pair as φ_{ia} and φ_{ib}.

Calculations are most conveniently carried out in an orthogonal basis of orbitals and so GVB calculations usually impose a second approximation, the *strong orthogonality* (SO) approximation. Within that approximation[35] the orbitals of different electron pairs are restricted to be mutually orthogonal, while orbitals belonging to the same pair overlap to an extent determined in the self-consistent calculation, i.e., $S_{iajb}=\langle\varphi_{ia}|\varphi_{jb}\rangle\delta_{ij}$. For N-electron pairs, the approximate GVB wave function can be expanded in a set of $2N$ mutually orthogonal natural orbitals, ϕ_i, as

$$\Psi_{\text{SOPP-GVB}}=\mathcal{A}\{[(\phi_1\phi_1-\lambda_1^2\phi_1'\phi_1')(\phi_2\phi_2-\lambda_2^2\phi_2'\phi_2') \times(\phi_3\phi_3-\lambda_3^2\phi_3'\phi_3')\cdots](\alpha\beta\alpha\beta\alpha\beta\cdots)\} , \tag{3}$$

which can be readily transformed to overlapping (within pairs only) SOPP-GVB orbitals by the following relations:

$$\varphi_{ia}=\phi_i+\lambda_i\phi_i' \text{ and } \varphi_{ib}=\phi_i-\lambda_i\phi_i' . \tag{4}$$

This is a good approximation in many bonding situations since overlaps of orbitals within a pair are close to unity and are greater than overlaps between orbitals in different pairs.[36] When the SOPP-GVB wave function is expanded in the natural orbital representation as in the following:

$$\Psi_{\text{SOPP-GVB}}=\mathcal{A}[(\phi_1\phi_1\phi_2\phi_2\phi_3\phi_3\cdots-\lambda_1^2\phi_1'\phi_1'\phi_2\phi_2\phi_3\phi_3\cdots + \cdots)(\alpha\beta\alpha\beta\alpha\beta\cdots)] , \tag{5}$$

where the final ellipsis represents additional terms, the parallel between this method and the more general multiconfiguration self-consistent-field (MCSCF) method is made clear. The SOPP-GVB wave function contains all double, quadrupole, hextuple, . . . , N-tuple excitations out of the HF configuration, with the constraint on the configuration coefficients that they be products of λ_i^2 and that individual pairs in the GVB representation [i.e., using Eq. (4)] should remain normalized. The orbitals and constrained configuration coefficients of the SOPP-GVB wave function are optimized to yield a self-consistent wave function with the lowest energy.

The third approximation that is made in this work is to neglect correlation of core electrons and represent them as a product of doubly occupied (HF) orbitals or to replace the core electrons by an effective core potential[37] (ECP). The actual all-electron SOPP-GVB wave function used in our computations is given by

$$\Psi_{\text{SOPP-GVB}}=\mathcal{A}\{(C)[\varphi_{1a}\varphi_{1b}\varphi_{2a}\varphi_{2b}\varphi_{3z}\varphi_{3b}\cdots] \times[(\alpha\beta-\beta\alpha)(\alpha\beta-\beta\alpha)(\alpha\beta-\beta\alpha)\cdots]\} , \tag{6}$$

where (C) is a product of doubly occupied HF orbitals representing the core electrons of the system. Note that the further restriction that enforces unit overlap of orbitals within pairs (i.e., $S_{iajb}=\delta_{ab}\delta_{ij}$) results in the Hartree-Fock wave function for the system. Hence, the SOPP-GVB wave function may be regarded as a generalization of the Hartree-Fock wave function. The orbitals of a HF wave function can be transformed from the canonical molecular orbitals to localized molecular orbitals or other forms by arbitrary unitary transformations without changing the energy of the system. By contrast, the localized orbitals of a GVB wave function are unique since that wave function consists of more than one Slater determinant and there is no unitary transformation between one set of GVB orbitals and another; any change in the self-consistently determined optimum GVB orbitals *will cause the energy of the system to increase.*

It is important, when possible, to include intrapair-correlation effects in calculating equilibrium geometries of silicon clusters, because "stretched" and "bent" bonds are two of their primary features. Intrapair-correlation effects are particularly important in "stretched" covalent bonds, because the overlap of the orbitals in the bond differs significantly from unity as the bond is stretched. As just noted, this overlap is determined self-consistently in the GVB wave function but is always restricted to unity in the HF wave function. Therefore the HF wave function necessarily has a large *correlation error* when spin-paired orbitals should overlap to only a small extent. There are especially important correlation effects associ-

ated with long bonds in silicon clusters since they have overlaps of only ~0.6 in their equilibrium geometries. Hence to obtain correct long-bond distances and relative energies for clusters with different structures and differing numbers of long bonds these correlation effects are crucial. As an example, Si_{10}, which is described in detail in the next section, is found to have a TBN structure and a PBN structure within 0.01 eV of each other using GVB calculations. Using the Hartree-Fock wave functions, the TBN cluster is found to be 2.62-eV higher in energy than the PBN cluster! This results from the inability of the HF wave function to adequately describe the four long bonds of the TBN cluster.

The work presented here is based on a valence-bond (VB) point of view that is distinct from all other theoretical studies on silicon clusters reported thus far. Whether they have included electron correlation or not, they all have been based on *molecular-orbital* methods. The present VB model is based on *localized* orbitals and intrapair correlations are explicitly included in the calculations. When molecular orbitals or Bloch states are chosen as the basis for a description of the electronic structures of clusters or the solid, respectively, the symmetry of the entire system is emphasized in the orbitals. By contrast, a localized orbital description emphasizes distributions of electrons on a length scale comparable to internuclear separations, which gives an alternative perspective on the relationship between bonding in clusters and solids. Just as it is possible to transform canonical Hartree-Fock molecular orbitals to localized molecular orbitals, delocalized Bloch states may be transformed to localized Wannier states. The latter approach has been followed by Fulde and co-workers.[38] In their method, which they refer to as the "local approach," they treat electron correlations, in bulk diamond and silicon within a basis of bond-centered, localized Wannier orbitals and consider correlations over a range of at most two bond distances. For diamond[38(b)] they showed that the dominant correlations in the ground state are within a bond (i.e., between a pair of electrons localized within an internuclear region) and between nearest-neighbor bonds; the contribution to the total energy of the correlations within a bond being the larger of the two. Longer-range correlations were found to contribute negligibly to the total energy.[38(b)] More recently the local approach has been applied to excitations in diamond and silicon and found to give direct band gaps and bandwidths in good agreement with experiment.[38(c),38(d)]

III. RESULTS OF COMPUTATIONS FOR CLUSTERS WITH 3–10 ATOMS

A. Si_5

The equilibrium structure for the five-atom clusters has been found to be a trigonal bipyramid with D_{3h} symmetry that has a $^1A_1'$ ground state.[17,20,21,24] We also obtain this structure but further conclude (see Fig. 3) that the cluster contains six bent bonds, one long bond, and three angularly correlated lone pairs and is therefore a TBN cluster. Two of the bent bonds are shown schematically

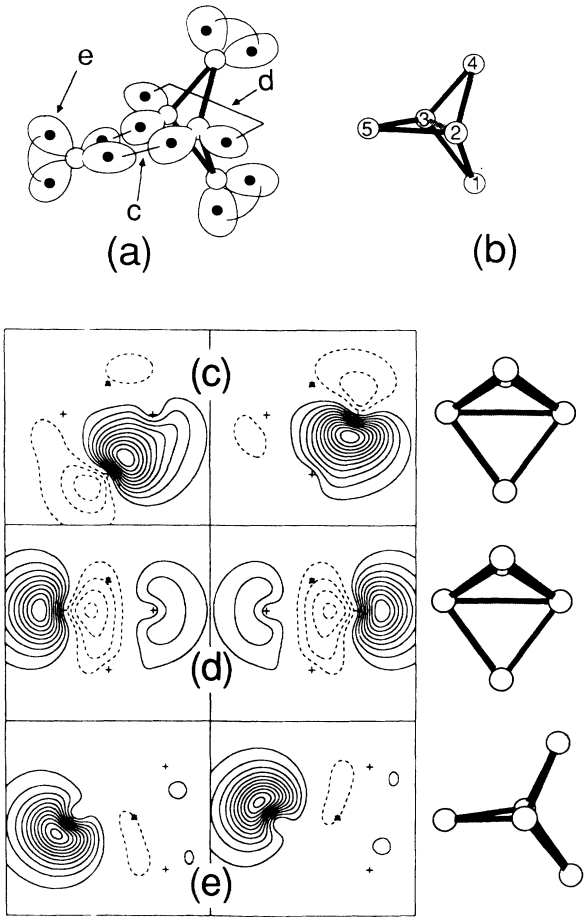

FIG. 3. Schematic diagrams of (a) GVB orbitals of TBN D_{3h} $^1A_1'$ Si_5 and (b) the molecular structure of Si_5. Bent bonds are indicated by a thick solid line and the long bond is indicated by a shaded line. Singlet pairing of orbitals is indicated by thin solid lines. Also shown are contour plots of GVB orbitals representing (c) a bent bond, (d) the long bond, and (e) an angularly correlated lone pair. In these contour plots and all others, the contours are separated by 0.02 a.u. and the initial contour is 0.02 a.u.; + indicate atoms in the plane of the paper; × and △, respectively, indicate atoms in front of and behind that plane.

in Fig. 3(a) as pairs of singlet-coupled orbitals (the coupling is denoted by thin lines) on Si(2) and Si(5), and Si(3) and Si(5), respectively. The remaining four bent bonds are shown as thick, solid lines. The long bond is formed by overlap of two orbitals on atoms 2 and 3 pointing in opposite direction along the principal axis of the cluster. Contour plots of SOPP-GVB orbitals corresponding to a bent bond, the long bond, and an angularly correlated lone pair in Si_5 are shown in Figs. 3(c)–3(e), respectively. We obtained equilibrium geometries for Si_5 using all-electron (AE) and effective-core-potential (ECP) calculations (see Appendix A) for both HF and GVB wave functions. Total energies for the ^3P ground state of the Si atom using HF and SOPP-GVB wave functions for both AE and ECP are given in Table I. The equilibrium bond

TABLE I. Total energies for the ^3P state of the Si atom.

Wave function	Basis set	Total energy (hartree)
HF	AE	−288.829 696
HF	ECP[a]	−288.829 509
GVB	AE	−288.842 938
GVB	ECP[a]	−288.843 326

[a]Effective core potential core energy = −285.154 934 (hartree).

lengths, bond angles, total energies, and cluster binding energies per atom for Si_5 are compared in Table II. From this point on we will use "GVB wave function" to refer to an SOPP-GVB wave function and will explicitly note whether an effective potential is used, e.g., GVB-AE refers to a SOPP-GVB calculation performed with all electrons.

The GVB-AE wave function gives an equilibrium distance for the bent bond of 2.39 Å, a long-bond distance of 2.79 Å, and a binding energy per atom of 1.85 eV/atom. The GVB-ECP wave function gives corresponding equilibrium bond distances of 2.39 and 2.81 Å, respectively, and a binding energy of 1.86 eV/atom. For a HF-AE (or HF/ECP) wave function, the bond lengths are 2.35 Å (2.35 Å) and 2.84 Å (2.86 Å) and the binding energy is 1.65 (1.73) eV/atom. These geometric parameters and binding energies may be compared to results obtained by Raghavachari[17] using HF wave functions with a more restricted basis set. He reports corresponding bond distances of 2.34 2.78 Å and a binding energy of 1.48 eV/atom for Si_5. The binding energies obtained with the AE basis set used in this work are typically 0.15 eV/atom greater (at the HF level) than those reported by Raghavachari.[17] These comparisons show that the ECP and AE calculations employed in this work give geometries and binding energies in good agreement with each other for both GVB or HF wave functions. A more extensive comparison of results is reserved for discussion in Appendix B.

Bent bonds are so named because the maxima of the probability amplitudes of the orbitals in the bond lie outside the bond axis [Fig. 3(c)]. They are generally slightly longer than colinear single bonds. Hence, the bent-bond distance predicted by the GVB-AE wave function is found to be 2.39 Å in Si_5, compared to 2.35 Å in the solid. However, the bent-bond distance of 2.35 Å predicted by the HF-AE wave function is too short. The long-bond distance of 2.79 Å (using the GVB-AE wave function) is rather typical of such bonds for these clusters. Because of the well-known incorrect asymptotic behavior of Hartree-Fock wave functions at large internuclear separations that leads to predicted bond lengths that are too short, one might naively expect the HF-AE wave function to predict a *shorter* long-bond distance than the GVB-AE wave function. However, the HF-AE wave function actually gives a long-bond distance 0.05-Å *longer* than the GVB-AE wave function. This can be explained in terms of the particular bonding situation in Si_5. The long-bond distance is determined by competition between strain in the bent bonds, which contributes a force tending to separate atoms 2 and 3, and the long bond that tends to bring atoms 2 and 3 closer. Hence the tendency for the HF wave function to predict bond distances that are too short results in six contracted bent-bond distances and the structure must compensate by giving slightly larger angles between bent bonds, which in turn results in a longer long-bond distance [this trend in Si(2)-Si(1)-Si(3) bond angles is observed for both calculations in Table II].

Long bonds are found in nearly all silicon clusters with 3–10 atoms, but are not unique to them. The stability of a hydrocarbon molecule with a very similar structure had been the subject of theoretical debate for many years[39] and was synthesized for the first time in 1982.[40] A tin analog of the hydrocarbon also has been synthesized recently[41] and thus compounds with long bonds have been identified in three of the group IV elements. The hydrocarbon [1.1.1] propellane (C_5H_6), has a D_{3h} structure in which each C atom replaces a Si atom in the Si_5 cluster. Each C atom has two hydrogen atoms bonded to it in the mirror plane perpendicular to the C_3 rotation axis, so each of the lone-pair electrons in Si_5 is replaced by a C—H bond in the hydrocarbon. Comparison of the results of a GVB calculation for [1.1.1] propellane[39(e)]

TABLE II. Total energies, equilibrium geometries, and cluster binding energies for Si_5.

Wave function	State	Total energy (hartree)	Bond length (Å)		Bond angle (deg)		Binding energy (eV/atom)
GVB-AE	$^1A_1'$	−1444.554 714	Si(1)—Si(2)	2.39	Si(2)-Si(1)-Si(3)	71.5	1.85
D_{3h} TBN cluster			Si(2)—Si(3)	2.79	Si(1)-Si(2)-Si(4)	89.3	
GVB-ECP	$^1A_1'$	−1444.558 062	Si(1)—Si(2)	2.39	Si(2)-Si(1)-Si(3)	72.1	1.86
D_{3h} TBN cluster			Si(2)—Si(3)	2.81	Si(1)-Si(2)-Si(4)	88.9	
HF-AE	$^1A_1'$	−1444.452 549	Si(1)—Si(2)	2.35	Si(2)-Si(1)-Si(3)	74.4	1.65
D_{3h} TBN cluster			Si(2)—Si(3)	2.84	Si(1)-Si(2)-Si(4)	87.2	
HF-ECP	$^1A_1'$	−1444.466 495	Si(1)—Si(2)	2.35	Si(2)-Si(1)-Si(3)	75.0	1.73
D_{3h} TBN cluster			Si(2)—Si(3)	2.86	Si(1)-Si(2)-Si(4)	86.8	
GVB-AE	$^3A_2''$	−1444.481 736	Si(1)—Si(2)	2.43	Si(2)-Si(1)-Si(3)	74.1	1.98[a]
D_{3h} TBN cluster			Si(2)—Si(3)	2.93	Si(1)-Si(2)-Si(4)	87.4	

[a]The singlet-triplet excitation energy is quoted instead of the cluster binding energy.

shows that GVB orbitals for the long bond in both compounds are similar.

In spite of the relatively low overlap (0.57) of the orbitals comprising the long bond in the GVB-AE wave function, the bond is quite "strong" and there is a significant change in the cluster structure when this bond is "absent." This is judged by considering the vertical and adiabatic singlet-triplet excitation energies to the $^3A_2''$ state and its equilibrium geometry. In that state electrons in the long-bond orbitals are triplet coupled and the wave function is antisymmetric with respect to the horizontal mirror plane. The GVB-AE vertical and adiabatic excitation energies are 2.09 and 1.98 eV, respectively. The equilibrium Si(2)-Si(3) distance is 2.93 Å and the bent-bond distance is 2.43 Å for the $^3A_2''$ state (Table II) compared to 2.79 and 2.39 Å in the ground state. This is not the lowest-energy triplet state for Si_5, however, as Raghavachari has found a $^3B_1$ state with C_{2v} symmetry, which is only 0.61-eV above the ground state.

B. Si_4

We began this section with the five-atom cluster because the three- and four-atom clusters may be derived from it by sequentially removing one or two atoms from the mirror plane perpendicular to the C_3 axis; this highlights the relationship between their VB descriptions. The C_{2v} structure of Fig. 4(a) illustrates the relationship between the four- and five-atom clusters; Si_4 may be obtained by removing Si(5) from Si_5, leaving a pair of dangling electrons on Si(2) and Si(3), which can either be singlet or triplet coupled. When they are singlet coupled the resulting ^1A_g ground state is planar with D_{2h} symmetry; triplet spin-coupling results in a higher total energy. Thus, as the schematic illustration in Fig. 4(b) shows, there are four bent bonds, a long bond, a π bond, and two angularly correlated lone pairs in Si_4. There is no unique face on the D_{2h} structure of Fig. 4(b), so the singlet-coupled pair of electrons may be found on either side of the cluster with equal probability. The GVB π orbitals in the planar geometry therefore represent a "mean-field" description of this electron pair. They are centered on Si(2) and Si(3) and so the π bond exists chiefly between these atoms. However, contour plots in a section perpendicular to the Si(2)—Si(4) bond and in a section slightly above the plane of the cluster [Fig. 4(c)] show that the π orbitals are rather more delocalized onto Si(1) and Si(4) than in their schematic depiction in Fig. 4(b). This delocalization results in shorter bonds of the type between Si(1)—Si(2), having lengths of 2.33 Å (Table III), compared to bent-bond lengths typically around 2.40 Å in clusters without π bonds. The long-bond distance in Si_4 for the GVB-AE wave function is 2.49 Å, much shorter than a typical long-bond distance; using the GVB-ECP wave function the equilibrium bond distances are 2.34 and 2.50 Å. The contracted Si(2)-Si(3) distance arises because *both* the long bond and the π bond exist between these atoms. Binding energies are given in Table III. Contour plots of the Si_4 long-bond orbitals, similar to the long-bond orbitals of Si_5, are shown in Fig. 4(d). When

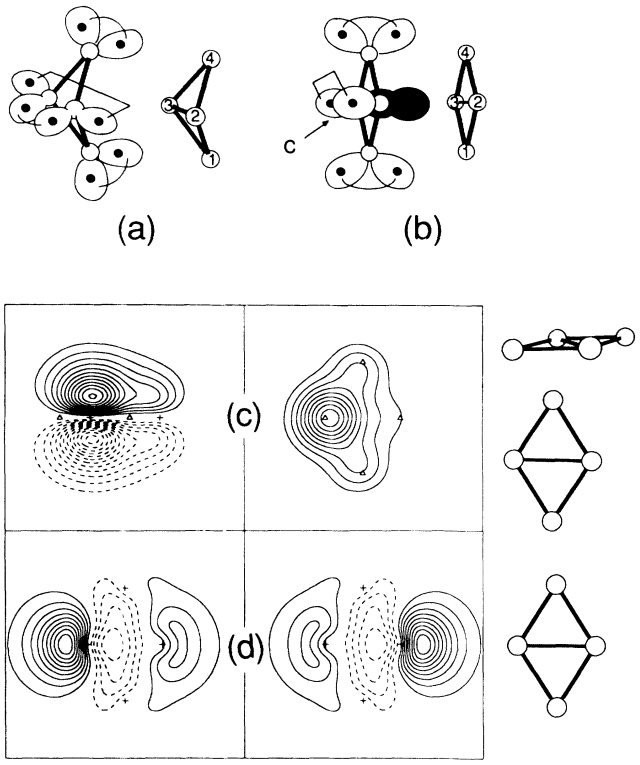

FIG. 4. Schematic diagrams and molecular structure of (a) C_{2v} $^1A_1$ Si_4 and (b) D_{2h} ^1A_g Si_4. The equilibrium geometry is the D_{2h} structure; (c) one of two symmetrically equivalent π-bond orbitals perpendicular to the molecular plane and along the line joining atoms 2 and 4 (left panel) and one of the π-bond orbitals parallel to the molecular plane but slightly above it (right panel); (d) the long-bond orbitals in the molecular plane.

the geometry optimization is carried out at the HF-AE level the bent-bond and long-bond–π-bond distances are 2.32 and 2.42 Å, respectively. For the HF-ECP wave function, the bond distances are 2.32 and 2.43 Å. These values may be compared to those obtained in previous studies of Si_4, which have been carried out at the HF (Ref. 17) and restricted complete active space self-consistent field (CASSCF) levels.[23] In the former case the equilibrium bond lengths were 2.30 and 2.40 Å and in the latter case the bond lengths were 2.29 and 2.39 Å. There are important correlation effects in both the long bond and the π bond of the ^1A_g state that lead to significant differences in equilibrium long-bond distances, depending on whether the GVB or HF wave functions are employed. The overlaps of the long bond and the π bond for the Si_4 GVB-AE wave function are 0.63 and 0.70, respectively, at the equilibrium bond lengths of the ^1A_g state. Such low overlaps (cf. $\sim$0.85 for bent bonds) mean that correlation effects cannot be neglected in obtaining accurate geometries for this molecule. It is a surprising result, therefore, to find that the equilibrium Si(2)—Si(3) bond distance obtained by the CASSCF method is actually shorter than either of the HF results mentioned above, in contrast to the longer distance obtained by the GVB

TABLE III. Total energies, equilibrium geometries, and cluster binding energies for Si_4.

Wave function	State	Total energy (hartree)	Bond length (Å)		Bond angle (deg)		Binding energy (eV/atom)
GVB-AE	^1A_g	−1155.638 892	Si(1)—Si(2)	2.33	Si(2)-Si(1)-Si(3)	64.5	1.82
D_{2h} TBN cluster			Si(2)—Si(3)	2.49	Si(1)-Si(2)-Si(4)	115.5	
GVB-ECP	^1A_g	−1155.637 893	Si(1)—Si(2)	2.34	Si(2)-Si(1)-Si(3)	64.7	1.80
D_{2h} TBN cluster			Si(2)—Si(3)	2.50	Si(1)-Si(2)-Si(4)	115.3	
HF-AE	^1A_g	−1155.560 225	Si(1)—Si(2)	2.32	Si(2)-Si(1)-Si(3)	62.9	1.64
D_{2h} TBN cluster			Si(2)—Si(3)	2.42	Si(1)-Si(2)-Si(4)	117.1	
HF-ECP	^1A_g	−1155.569 564	Si(1)—Si(2)	2.32	Si(2)-Si(1)-Si(3)	63.2	1.71
D_{2h} TBN cluster			Si(2)—Si(3)	2.43	Si(1)-Si(2)-Si(4)	116.8	

method. One significant difference between the GVB and CASSCF geometry optimizations is that no orbitals of a_2 symmetry (which are responsible for the correlation of the π bond in the GVB calculation) were included in the CASSCF active space.[23]

C. Si_3

Several *ab initio* theoretical studies of Si_3 already have been reported.[15,22,42] Results of these calculations agree that the $^1A_1$ ground state has C_{2v} symmetry and that there is a nearly degenerate $^3A_2'$ state with D_{3h} symmetry.[15,22,42b] We report results of GVB and HF calculations on the $^1A_1$ ground state only. It is generated by removing Si(4) from the D_{2h} ground state of Si_4, leaving a pair of dangling electrons that had participated in the bent bonds to Si(4). For the ground state of Si_3, spin coupling of just the dangling electrons left after removing Si(4) is not the only effect (as it was in forming Si_4 from Si_5). Here the long-bond orbitals are also involved in the recoupling of electron spins. When the wave function is fully optimized it is found that two new angularly correlated lone pairs are generated on Si(2) and Si(3) in the molecular plane and the long bond has been removed. The GVB orbitals for this molecule are shown schematically in Fig. 5(a). There are bent bonds between Si(1) and Si(2) and between Si(1) and Si(3) and lone pairs on all three atoms. In Si_3, the π bond can only delocalize onto Si(1) [cf. Si(1) and Si(4) in Si_4] and a much greater contraction is found in the Si(1)—Si(2) and Si(1)—Si(3) bond distances. The GVB-AE (or GVB-ECP) wave-function equilibrium bond distance is 2.22 Å (2.23 Å) and the bond angle is 80.0° (80.1°) (Table IV). The HF-AE (or HF-ECP) equilibrium bond distance is 2.17 Å (2.18 Å) and the bond angle is 78.2° (78.2°). These compare to previously reported values, using a HF wave function,[15] of 2.16 Å and 77.8°. Contour plots of the GVB π orbitals in sections perpendicular to the Si(1)—Si(2) bond and slightly above the molecular plane are shown in Fig. 5(b). There is very little π-orbital amplitude extending between Si(2) and Si(3); rather the π orbitals are almost exclusively delocalized in the direction of Si(1). That is to say, there is weak bonding between Si(2) and Si(3) but there are two one-electron bonds between Si(1) and Si(2) and Si(1) and Si(3). Therefore an interesting parallel arises between the VB descriptions of the electronic structures of the ground states of Si_3 and O_3 (ozone).[43] The bond length in ozone is 1.28 Å (Ref. 44), which is much shorter than a normal oxygen-oxygen single-bond length such as in hydrogen peroxide [1.47 Å (Ref. 45)]. Contour plots of the lone-pair orbitals on Si(3) are shown in Fig. 5(c). Note the large degree of angular separation that is a characteristic of the lone pairs found in these Si clusters.

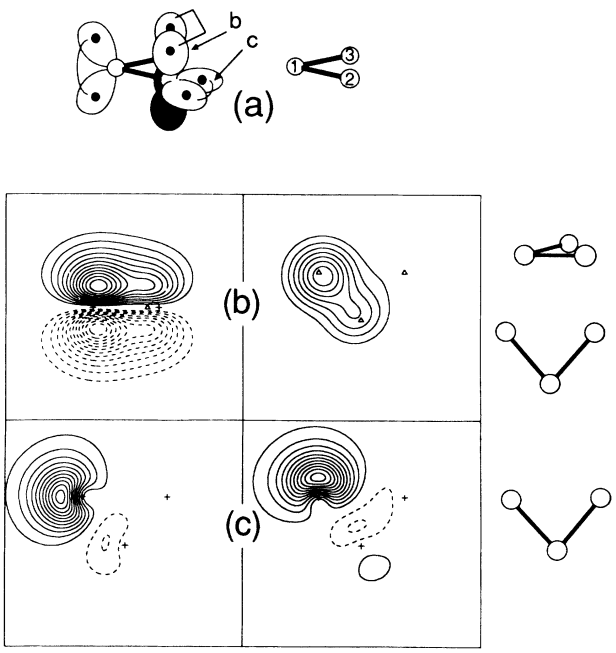

FIG. 5. (a) Schematic diagram and molecular structure of C_{2v} $^1A_1$ Si_3; (b) one of two symmetrically equivalent π-bond orbitals perpendicular to the molecular plane and along the line joining atoms 1 and 2 (left panel) and one of the π-bond orbitals parallel to the molecular plane but slightly above it (right panel); (c) angularly correlated lone-pair orbitals in the molecular plane.

D. Si_6

Geometry optimizations were performed with the GVB wave functions for four different structures of Si_6, and for comparison, the most stable cluster was also optimized for the HF wave function. Two of the Si_6 clusters

TABLE IV. Total energies, equilibrium geometries, and cluster binding energies for Si_3.

Wave function	State	Total energy (hartree)	Bond length (Å)		Bond angle (deg)		Binding energy (eV/atom)
GVB-AE C_{2v} TBN cluster	$^1A_1$	−866.676 480	Si(1)—Si(2)	2.22	Si(2)-Si(1)-Si(3)	80.0	1.34
GVB-ECP C_{2v} TBN cluster	$^1A_1$	−866.675 402	Si(1)—Si(2)	2.23	Si(2)-Si(1)-Si(3)	80.1	1.32
HF-AE C_{2v} TBN cluster	$^1A_1$	−866.617 515	Si(1)—Si(2)	2.17	Si(2)-Si(1)-Si(3)	78.3	1.16
HF-ECP C_{2v} TBN cluster	$^1A_1$	−866.623 596	Si(1)—Si(2)	2.18	Si(2)-Si(1)-Si(3)	78.2	1.22

studied are of the TBN class (TBN-I and TBN-II), a third (PBN-I) consists of a sixth atom bonded (*via* a three-center dative bond) to a fragment resembling the ground state of Si_5 and the fourth, and most stable cluster (PBN-II), has interstitial electron pairs. We find the relative stabilities of the latter two clusters to be the reverse of that reported by Raghavachari.[17] The PBN-II cluster is found to be the ground state for Si_6, with the PBN-I cluster lying 0.17-eV above it. Such low-lying states may result in fluxional behavior in these clusters (i.e., strong electronic-vibrational coupling resulting in exchanges of atomic positions in the cluster). Fluxional behavior is a well-established feature of many transition-metal cluster compounds.[45]

The TBN clusters, TBN-I and TBN-II, are shown in Figs. 6 and 7, respectively. The first is found to lie 2.17-eV and the second 0.42-eV above the ground state. The C_{2v} structure of TBN-I in Fig. 6 is generated by breaking the Si(2)—Si(5) bond in Si_5 and forming bent bonds between a sixth atom and Si(2) and Si(5). The tetrahedral

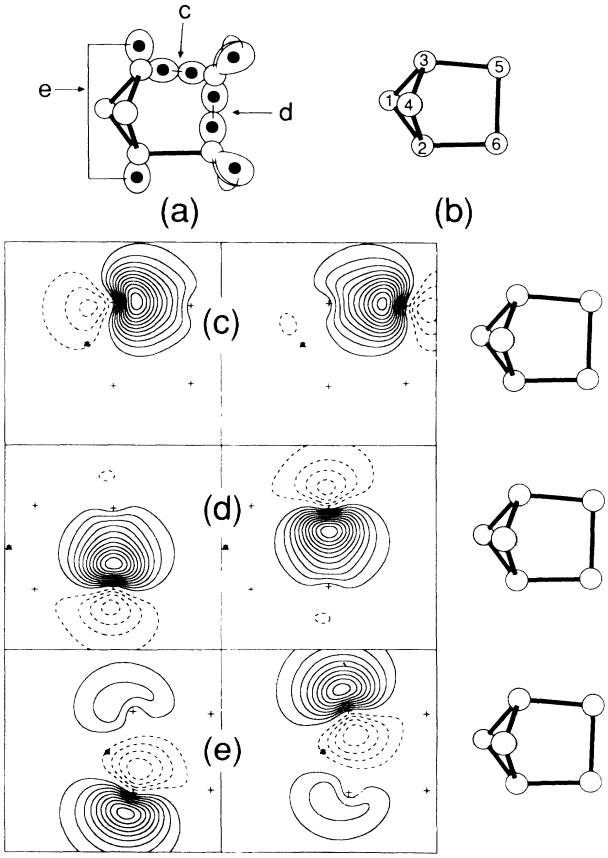

FIG. 6. (a) Schematic diagram and (b) molecular structure of TBN C_{2v} $^1A_1$ Si_6; bent-bond orbitals forming (c) the Si(3)—Si(5) and (d) the Si(5)—Si(6) bonds; (d) long-bond orbitals forming the Si(2)—Si(3) bond.

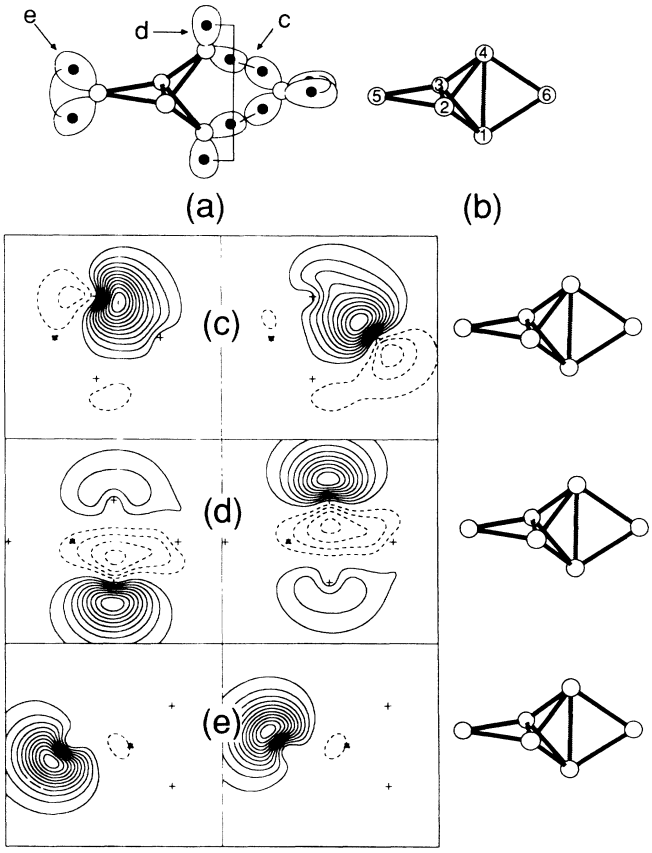

FIG. 7. (a) Schematic diagram and (b) molecular structure of TBN D_{2d} $^1A_1$ Si_6; (c) bent-bond orbitals forming the Si(4)—Si(6) bond; (d) long-bond orbitals forming the Si(1)—Si(4) bond; (e) lone-pair orbitals on Si(5).

TABLE V. Total energies, equilibrium geometries, and cluster binding energies for Si_6.

Wave function	State	Total energy (hartree)	Bond length (Å)		Bond angle (deg)		Binding energy (eV/atom)
GVB-ECP	$^1A_1$	−1733.412 572	Si(1)—Si(2)	2.37	Si(1)-Si(3)-Si(4)	95.0	1.60
			Si(2)—Si(3)	2.79	Si(2)-Si(4)-Si(3)	71.1	
C_{2v} TBN cluster			Si(2)—Si(6)	2.47	Si(3)-Si(5)-Si(6)	92.1	
			Si(5)—Si(6)	2.61	Si(4)-Si(3)-Si(5)	108.8	
GVB-ECP	$^1A_1$	−1733.476 886	Si(1)—Si(2)	2.36	Si(1)-Si(2)-Si(4)	97.9	1.89
			Si(2)—Si(3)	2.74	Si(2)-Si(4)-Si(3)	71.7	
D_{2d} TBN cluster			Si(2)—Si(5)	2.45	Si(2)-Si(5)-Si(3)	68.0	
	$^1A_1$	−1733.339 611	GVB geometry				1.64
GVB-ECP	$^1A_1$	−1733.485 792	Si(1)—Si(2)	2.46	Si(1)-Si(2)-Si(4)	105.0	1.93
			Si(1)—Si(6)	2.39	Si(1)-Si(2)-Si(5)	84.2	
C_{2v} PBN cluster I			Si(2)—Si(3)	2.69	Si(1)-Si(6)-Si(4)	108.8	
			Si(2)—Si(5)	2.34	Si(2)-Si(4)-Si(3)	66.6	
					Si(2)-Si(4)-Si(6)	60.5	
					Si(2)-Si(5)-Si(3)	70.2	
GVB-ECP	$^1A_1$	−1733.492 236	Si(1)—Si(2)	2.39	Si(1)-Si(2)-Si(4)	91.5	1.96
			Si(2)—Si(3)	2.73	Si(1)-Si(2)-Si(6)	68.4	
C_{2v} PBN cluster II			Si(2)—Si(5)	2.51	Si(2)-Si(1)-Si(3)	69.7	
(three-center–			Si(5)—Si(6)	2.35	Si(2)-Si(5)-Si(3)	66.0	
two-electron bonds)					Si(2)-Si(5)-Si(6)	62.1	
					Si(5)-Si(2)-Si(6)	55.9	
HF-ECP	$^1A_1$	−1733.384 912	Si(1)—Si(2)	2.37	Si(1)-Si(2)-Si(4)	93.0	1.85
			Si(2)—Si(3)	2.70	Si(1)-Si(2)-Si(6)	67.6	
C_{2v} PBN cluster II			Si(2)—Si(5)	2.46	Si(2)-Si(1)-Si(3)	68.8	
(three-center–			Si(5)—Si(6)	2.36	Si(2)-Si(5)-Si(3)	66.1	
two-electron bonds)					Si(2)-Si(5)-Si(6)	61.7	
					Si(5)-Si(2)-Si(6)	56.5	

arrangement of VB orbitals in this cluster is shown schematically in Fig. 6(a); angularly correlated lone pairs on Si(1) and Si(4) are not shown in the schematic diagram. Bond lengths and angles for the GVB-ECP optimized geometry are given in Table V. Bent-bond distances are 2.37, 2.47, and 2.61 Å and the long-bond distance is 2.79 Å. The shortest bent bond (2.37 Å) is a typical bent-bond distance but the longer bent-bond distances (2.47 and 2.61 Å) are abnormally long. We find that longer bent bonds subtend larger angles between bonds when there is an angularly correlated lone pair on the atom between the bonds. Contour plots of orbitals representing the Si(3)—Si(5) bond (2.47 Å), the Si(5)—Si(6) bond (2.61 Å), and the Si(2)—Si(3) long bond are shown in Figs. 6(c)–6(e). This open structure has a low-binding energy (1.60 eV/atom at the GVB-ECP level) and is the least stable of the four structures.

The TBN-II cluster with D_{2d} symmetry may be generated by bonding an extra atom to the Si_5 cluster in a different way. The lone pairs on Si(1) and Si(4) (Fig. 3) are recoupled so that bent bonds are formed between Si(6) and atoms Si(1) and Si(4) and a long bond is formed between Si(2) and Si(3) [Fig. 7(a)]. The GVB-ECP optimized geometry has bond lengths of 2.34, 2.45 (bent bonds), and 2.74 Å (long bonds). Contour plots of orbitals representing the Si(4)—Si(6) bent bond, the Si(1)—Si(4) long bond, and the angularly correlated lone pair on Si(5) are shown in Figs. 7(c)–7(e), respectively.

The PBN-I cluster with a three-center dative bond and C_{2v} symmetry (see Table V) is illustrated in Fig. 8(a). It is comprised of a Si_5 cluster with Si(1) and Si(4) distorted somewhat to allow a sixth atom to form a three-center dative bond to Si(1) and Si(4). Contour plots of the dative bond orbitals and the lone pair on Si(4) are shown in Figs. 8(c) and 8(d). Optimized bond lengths at the GVB-ECP level were 2.34, 2.46 (bent bonds), 2.39 (dative bond), and 2.69 Å (long bond). This structure is 0.17-eV above the ground-state energy.

The ground-state structure for Si_6 (PBN-II) also has a C_{2v} symmetry. It may be generated from Si_5 by replacing Si(1) in Si_5 by a pair of atoms—Si(1) and Si(6) in Fig. 9(b). The structure is also related to PBN-I above by rotating atoms 1 and 6 clockwise about the Si(2)-Si(3) axis by about 20°. A schematic representation of the bonding for the PBN-II cluster is shown in Fig. 9(a). Atoms Si(2) and Si(3) have a tetrahedral arrangement of four orbitals about them and Si(4) and Si(5) have bonding environments similar to that in Si_5. Atoms Si(2) and Si(3) have orbitals pointing away from each other along the Si(2)-Si(3) axis forming a long bond [these are omitted from Fig. 9(a)] and three more orbitals that either form bent bonds to atoms 1 and 4 or contribute to the interstitial orbitals in the triangular faces Si(2)-Si(1)-Si(6) and Si(3)-Si(1)-Si(6). One of the latter GVB orbitals that is part of

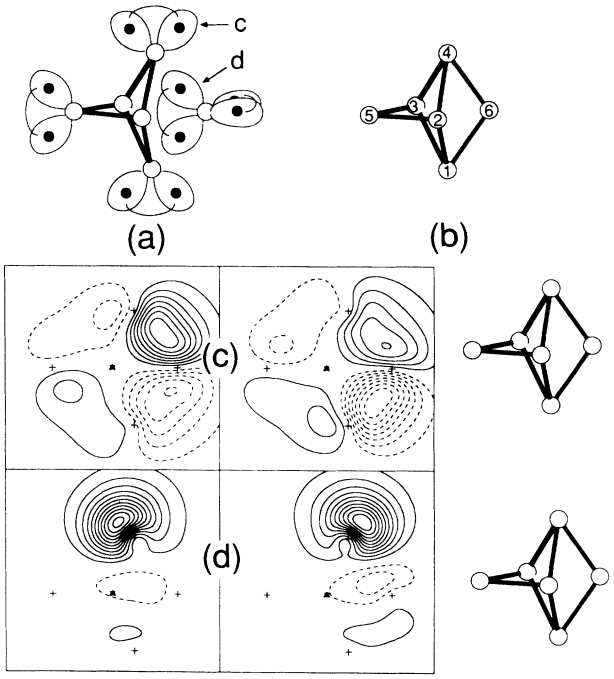

FIG. 8. (a) Schematic diagram and (b) molecular structure of PBN C_{2v} $^1A_1$ Si_6; (c) orbitals forming the Si(1)—Si(6)—Si(4) dative bond; (d) lone-pair orbitals on Si(4).

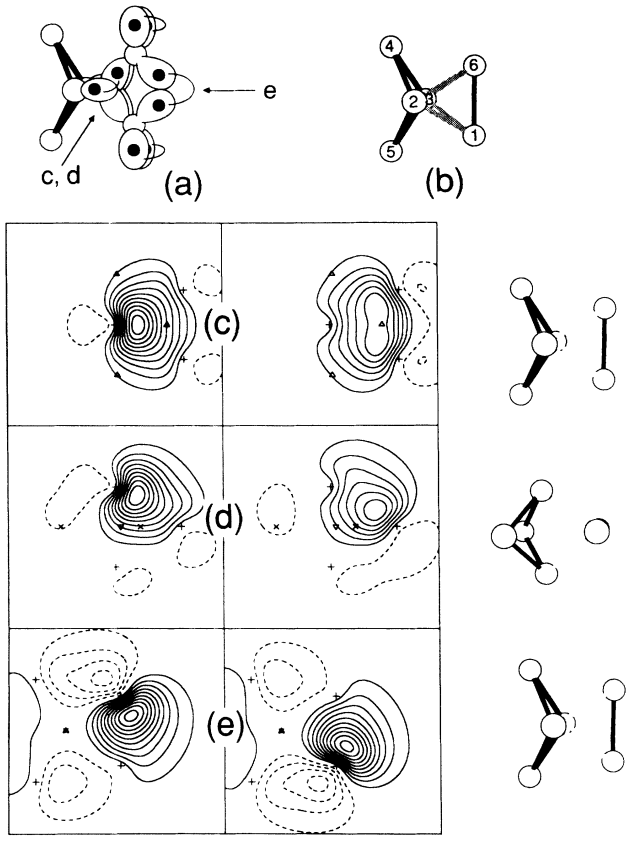

FIG. 9. (a) Schematic diagram and (b) molecular structure of PBN C_{2v} $^1A_1$ Si_6; (c) orbitals forming the Si(2)—Si(1)—Si(6) interstitial pair; (d) the same interstitial pair orbitals in a plane containing Si(2), Si(1), and Si(3); (e) orbitals forming the Si(1)—Si(6) bond.

an interstitial pair is shown in the left panel of Fig. 9(c). A plot of the interstitial pair orbitals through the Si(2)-Si(1)-Si(6) plane is shown in Fig. 9(d) to demonstrate that the interstitial pair is actually localized in this face. There is also a bond between Si(1) and Si(6) that is shown in Fig. 9(e). This description and the schematic diagram in Fig. 9(a) show that atoms Si(1) to Si(4) have *four* orbitals each in a tetrahedral arrangement, but atoms Si(5) and Si(6) have *five* orbitals on each of them, although some of these (the interstitial pair orbitals) are also shared between two atoms. Equilibrium bond lengths at the GVB-ECP level are 2.35, 2.39 (bent bonds), 2.51 (interstitial pairs), and 2.71 Å (long bond).

The importance of correlating long bonds in obtaining accurate relative energies for clusters with different numbers of long bonds is illustrated by comparing differences in total energy at the HF and GVB levels between the clusters illustrated in Fig. 7 (with two long bonds) and Fig. 9 (with one long bond). At the HF level the cluster with two long bonds is 1.23-eV above the cluster with one long bond but at the GVB level this energy difference is reduced to 0.42 eV. The reason for this large difference is simply that the GVB correlation energy for a long bond is much larger ($\sim$1.0 eV) than the correlation energy for a bent bond ($\sim$0.3 eV) or a lone pair and this illustrates the importance of correlating long bonds in obtaining reliable relative total energies for these clusters. We made this point above and will see it again later, but its importance deserves the emphasis we place on it.

E. Si_7

Three seven-atom clusters were studied: two of these are PBN clusters and one is a TBN cluster. The PBN clusters are: a tricapped trigonal pyramid[19] (TTP) (Fig. 10) and a pentagonal bipyramid[19,20,21] (PB) (Fig. 11), which is the HF ground-state structure for Si_7. The tricapped trigonal pyramid is better described as a monocapped, puckered six-atom ring from the point of view of its bonding as revealed by the GVB orbitals and HF localized molecular orbitals—but we retain the name that was first given to it in the literature. The TBN cluster has C_{2v} symmetry and is shown schematically in Fig. 12(a); it may be viewed as a six-atom cluster (Fig. 7) in which a seventh atom has been inserted between Si(1) and Si(6). It is expected to be the lowest-energy Si_7 TBN cluster. The structures of all three clusters were optimized at the HF-ECP level and GVB-ECP calculations were performed at the HF-ECP equilibrium geometry in order to evaluate the relative importance of intrapair correlation for these clusters and obtain a binding energy including electron correlation. Total energies, geometrical parameters, and cluster binding energies per atom are given in Table VI.

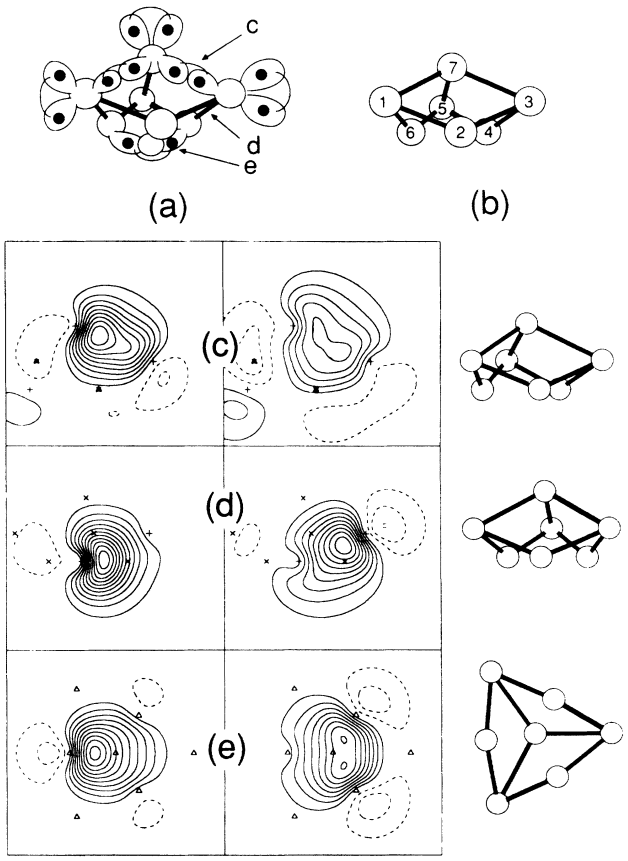

FIG. 10. (a) Schematic diagram and (b) molecular structure of PBN C_{3v} $^1A_1$ Si_7; (c) orbitals forming the Si(3)—Si(7) bond pair; (d) orbitals forming the Si(2)—Si(3) bond pair; (e) orbitals forming the Si(2)-Si(4)-Si(6) interstitial pair.

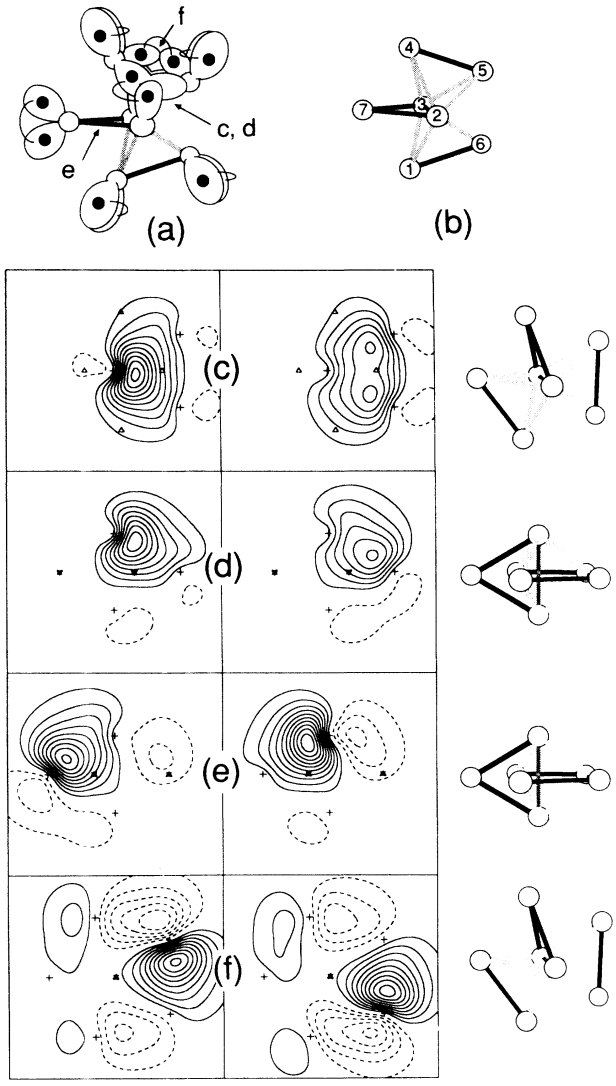

FIG. 11. (a) Schematic diagram and (b) molecular structure of PBN D_{5h} $^1A_1'$ Si_7; (c) orbitals forming the Si(2)-Si(4)-Si(5) interstitial pair; (d) the same interstitial pair orbitals in a plane containing Si(2), Si(3), and Si(6); (e) orbitals forming the Si(2)—Si(7) bent-bond pair; (f) orbitals forming the Si(4)—Si(5) bond pair.

The tricapped trigonal pyramid is a higher-energy structure than the pentagonal bipyramid, in agreement with the results of previous studies.[19] The bonding description for the TTP cluster is shown schematically in Fig. 10(a). The bonding orbitals participate in six bent bonds in the six-membered ring and three additional bent bonds among the three upper atoms in the ring [Si(1), Si(3) and Si(5)] and the capping atom [Si(7)]. There is also an interstitial pair localized among the three lower atoms in the ring [Si(2), Si(4), and Si(6)]. The remaining nonbonding lone pairs are localized on atoms Si(1), Si(3), Si(5), and Si(7). Thus there are five atomiclike orbitals localized on the latter atoms and three on the atoms Si(2), Si(4), and Si(6). Contour plots of GVB pairs corresponding to a bent bond between the ring and the capping atom, a bent bond in the ring and the interstitial pair are shown in Figs. 10(c)–10(e), respectively. This monocapped structure is ~0.5 eV/atom more stable than the uncapped, puckered six-membered ring: the binding energies for the monocapped ring and the uncapped, puckered ring have been reported previously as 1.72 (Ref. 18) and 1.23 eV/atom,[17] respectively. Why should the monocapped ring be so much more stable than the uncapped ring? The uncapped ring contains six bent bonds and six

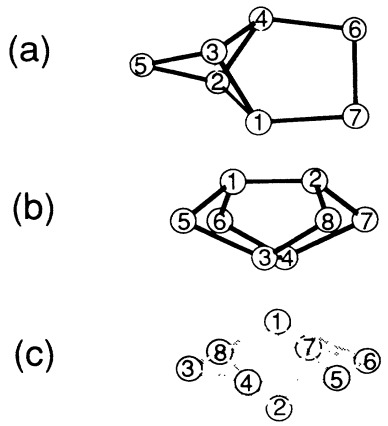

FIG. 12. Molecular structures for (a) TBN C_{2v} Si_7; (b) TBN D_{2d} Si_8; (c) PBN D_{6h} Si_8.

lone pairs, whereas the monocapped ring contains nine bent bonds, one interstitial pair and four lone pairs. The much higher ratio of bond pairs to nonbonding lone pairs in the monocapped ring (10:4 versus 6:6) results in a significantly greater stability in that case. Bond lengths, bond angles, and binding energies per atom for all seven-atom clusters are given in Table VI.

The pentagonal bipyramid structure is related to the equilibrium structure for Si_6. In the latter structure (Fig. 9) two atoms [Si(4) and Si(5)] are bonded to the axial atoms [Si(2) and Si(3)] by two-center–two-electron bonds. The other two [Si(1) and Si(6)] are bonded to the axial atoms [Si(2) and Si(3)] by three-center–two-electron $(3c,2e)$ bonds (interstitial pairs); there are four orbitals on the axial atoms. In the structure for Si_7 (Fig. 11), one atom [Si(7)] is bonded to the axial atoms [Si(2) and Si(3)] by $(2c,2e)$ bonds and two pairs of atoms [Si(1 and 6) and Si(4 and 5)] are bonded to the axial atoms [Si(2) and Si(3)] *via* interstitial pairs; there are still four tetrahedrally oriented orbitals on the axial atoms.

At the HF-ECP level the pentagonal bipyramidal structure has bond lengths of 2.50 Å between nearest-neighbor atoms in the horizontal mirror plane and 2.50 Å between atoms in the plane and on the fivefold rotation axis and a long-bond length of 2.61 Å between atoms on the rotation axis. The VB network derived from a GVB-ECP calculation at the HF-ECP equilibrium geometry is shown schematically in Fig. 11(a). As was mentioned above, atoms on the rotation axis have an approximately tetrahdral arrangement of four orbitals. Two orbitals on each of Si(2) and Si(3) point into the four triangular faces [Si(2)-Si(4)-Si(5), Si(2)-Si(1)-Si(6), Si(3)-Si(4)-Si(5), Si(3)-Si(1)-Si(6)]. One of these equivalent orbitals in the Si(2)-Si(4)-Si(5) face is shown in the left panel of Fig. 11(c). The other orbital of the pair is chiefly localized on Si(4) and Si(5) [right panel of Fig. 11(c)]. A section through this pair in the Si(2)-Si(3)-Si(6) plane shows that this pair is indeed localized in the triangular face. The fourth orbital localized on Si(2) or Si(3) is oriented towards Si(7) and forms part of a $(2c,2e)$ bond to that atom [Fig. 11(e)]. Finally, there are also bond pairs chiefly localized between Si(1) and Si(6) and between Si(4) and Si(5). One of these is shown in Fig. 11(f). Note that there is considerable delocalization of this pair into the region where no bond is indicated in the schematic diagram of Fig. 11(a). Thus atoms Si(2), Si(3), and Si(7) have four approximately tetrahedrally localized orbitals about them, whereas the remaining atoms have five localized atomiclike orbitals.

There is one further important point to be made about this cluster. The geometry optimization was carried out at the HF level and resulted in a structure with D_{5h} symmetry. The GVB wave function described above, on the other hand, has C_{2v} symmetry. Hence it is not clear whether a RVB description involving five resonance structures is more stable than a distorted pentagonal bipyramid with C_{2v} symmetry. In the latter case, correlation effects (which are not included in the HF wave function) would be responsible for the symmetry breaking. Without performing an RVB (or an approximately equivalent CI or MCSCF) calculation including dynamical correlation effects it is impossible to decide whether the equilibrium geometry of this cluster has D_{5h} or C_{2v} symmetry.

The Si_7 TBN cluster is shown schematically in Fig. 12(a). It may be formed by recoupling the lone pairs on Si(1) and Si(4) in the Si_6 cluster shown in Fig. 6 to form bent bonds to a seventh atom. The cluster has bent-bond lengths of 2.34, 2.40, 2.50, and 2.50 Å; the longest bonds join Si(6) and Si(7) to one another and to the remainder of the cluster. Long-bond lengths in the cluster are 2.74 Å [Si(2)-Si(3)] and 3.00 Å [Si(1)-Si(4)]. GVB orbital plots for this cluster are not shown since orbitals for the long

TABLE VI. Total energies, equilibrium geometries, and cluster binding energies for Si_7.

Wave function	State	Total energy (hartree)	Bond length (Å)		Bond angle (deg)		Binding energy (eV/atom)
HF-ECP	$^1A_1$	−2022.211 015	Si(1)–Si(2)	2.34	Si(1)-Si(2)-Si(4)	79.4	1.57
			Si(1)—Si(4)	3.00	Si(1)-Si(2)-Si(5)	94.3	
C_{2v} TBN cluster			Si(1)—Si(7)	2.50	Si(2)-Si(1)-Si(7)	115.7	
			Si(2)—Si(3)	2.74	Si(2)-Si(4)-Si(3)	71.7	
			Si(2)—Si(5)	2.40	Si(2)-Si(5)-Si(3)	69.5	
			Si(6)—Si(7)	2.50	Si(4)-Si(6)-Si(7)	95.6	
GVB-ECP	$^1A_1$	−2022.363 302	HF geometry				1.75
HF-ECP	$^1A_1$	−2022.288 414	Si(1)—Si(2)	2.33	Si(1)-Si(2)-Si(3)	131.7	1.87
			Si(1)—Si(7)	2.74	Si(1)-Si(6)-Si(2)	57.5	
C_{3v} PBN cluster			Si(2)—Si(4)	2.50	Si(2)-Si(1)-Si(6)	65.0	
			Si(2)—Si(7)	2.57	Si(2)-Si(6)-Si(7)	61.0	
					Si(2)-Si(7)-Si(6)	58.0	
GVB-ECP	$^1A_1$	−2022.395 062	HF geometry				1.91
HF-ECP	$^1A_1'$	−2022.307 265	Si(1)—Si(2)	2.50	Si(1)-Si(2)-Si(6)	61.0	1.95
			Si(1)—Si(6)	2.50	Si(1)-Si(6)-Si(2)	58.9	
D_{5h} PBN cluster			Si(2)—Si(3)	2.62	Si(1)-Si(7)-Si(4)	108.0	
					Si(2)-Si(1)-Si(3)	58.9	
GVB-ECP	$^1A_1'$	−2022.412 386	HF geometry				1.98

bonds and bent bonds resemble those in Figs. 6 and 13. This cluster is of particular interest because a motif consisting of this cluster may be used to tile the unreconstructed Si(111) surface to form the (7×7) reconstructed surface. The cluster [Fig. 12(a)] contains both the dimer [Si(6) and Si(7)] and adatom [Si(2)] that are prominent features of that surface. The lone pairs of the embedded clusters are recoupled to form bonds to other surface atoms (some of the atoms in the reconstructed surface actually belong to two overlapping embedded clusters) and several TBN atoms must be added to complete the structure. In a later section, distances in the cluster are compared to surface experimental bond lengths derived from low-energy electron diffraction (LEED) experiments.

F. Si_8

Several structures previously have been considered for the eight-atom cluster including a monocapped-pentagonal bipyramid,[18] a bicapped octahedron,[18,24] a distorted bicapped octahedron,[18,20] a bicapped-trigonal prism,[18] and a structure of lower symmetry[18] (C_{2v}). We have optimized the most stable of these (the distorted bicapped octahedron) and three others that were suggested by theoretical insight obtained from calculations on the smaller clusters. Of these we find that the most stable structures resemble two Si_4 units bonded together either in a tetrahedral or polyhedral bonding network. We describe the TBN cluster first.

The equilibrium structure for Si_8 and its VB structure are illustrated in Fig. 13; the cluster has D_{2h} symmetry. It is the ground state equilibrium structure at the GVB level and has not been reported previously. If it is regarded as a pair of Si_4 clusters bonded together, each π pair in the two Si_4 units is now recoupled to form two bent bonds joining Si(2 and 6) and Si(3 and 7). There are bent-bond distances of 2.38 Å [Si(1)-Si(2)] and 2.44 Å [Si(2)-Si(6)] and there are long-bond distances of 2.65 Å at the HF-ECP equilibrium geometry (Table VII). Plots of GVB orbitals representing these three bonds are shown in Figs. 13(c)–13(e), respectively. The noncolinear long bond in Fig. 13(e) arises because the long-bond orbitals are approximately perpendicular to the planes containing Si(1), Si(4), and Si(6) and Si(1), Si(4), and Si(7).

Alternatively, in the PBN Si_8 cluster, the two four-atom units are joined by bonds between atoms Si(1 and 8) and Si(4 and 5) [Figs. 14(a) and 14(b)]. Atoms Si(1), Si(4), Si(5), and Si(8) have five localized orbitals and the remaining atoms have three localized orbitals. GVB orbital plots corresponding to the three unique bent-bond pairs in the cluster are shown in Figs. 14(c)–14(e). Long bond between Si(2 and 3) and Si(6 and 7) are not plotted. The cluster has C_{2h} symmetry and was found to be the equilibrium ground-state geometry by two other groups.[18,20] At the GVB level it is 0.08-eV *above* the D_{2h} structure but at the HF level (this work) is it 1.27-eV *below* the D_{2h} structure. Again, there are important correlation effects neglected by the mean-field methods (such as HF or LDF) contributing to this energetic discrepancy. First, the correlation effects in the long bonds of the TBN cluster are very important as the long-bond distance in that cluster is 0.16-Å longer than in the PBN cluster. Second, the energetic lowering from correlation of the lone pairs is greater in the TBN cluster because there are five orbitals localized on the atoms with lone pairs in the PBN cluster but only four in the TBN cluster; such correlation effects in molecular or solid-state systems generally become of greater importance as the electron density decreases. Together these correlation effects favor the TBN cluster by ~1.1 eV, the correlation of the lone pairs contributing the major part of this.

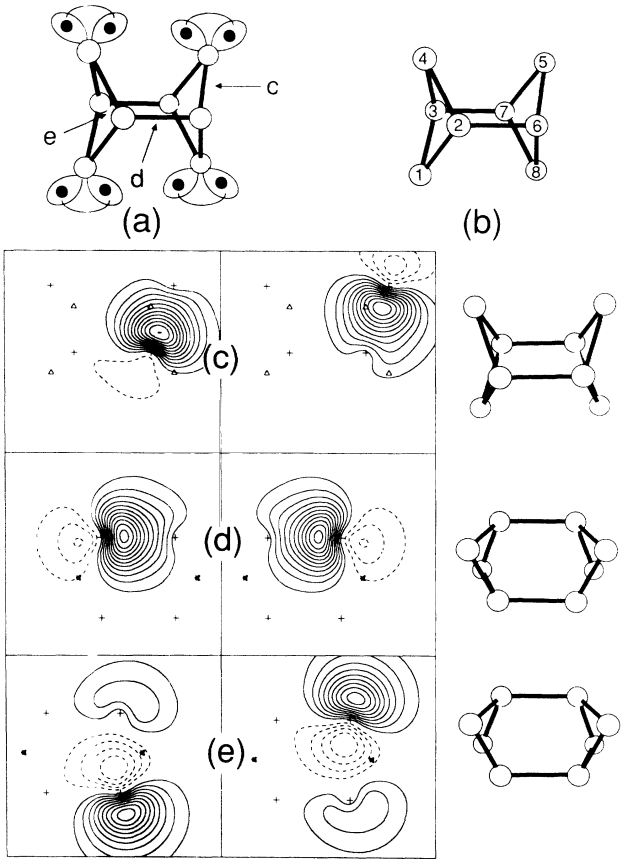

FIG. 13. (a) Schematic diagram and (b) molecular structure of ^1A_g D_{2h} TBN Si_8; (c) orbitals forming the Si(5)—Si(6) bent bond; (d) orbitals forming the Si(2)—Si(6) bent bond; (e) orbitals forming the Si(6)—Si(7) long bond.

The PBN cluster structure consists of two almost planar layers. The distances between planes are 2.60 Å [Si(1)-Si(8)] and 2.53 Å [Si(2)-Si(6)] so the atoms that are formally shown in Fig. 14(a) without a pair between them are actually closer than those with a bond pair! Further inspection shows that the pair in Fig. 14(e) is not a typical bent-bond pair; it delocalizes considerably inside the cluster and hence may be properly regarded as an interstitial pair localized in the tetrahedron Si(4)-Si(5)-Si(6)-Si(7). A contour plot of this pair in a plane containing Si(4), Si(6), and Si(7) [Fig. 14(f)] clearly demonstrates its interstitial character. There is an equivalent interstitial pair localized in the tetrahedron Si(1)-Si(2)-Si(3)-Si(8).

TABLE VII. Total energies, equilibrium geometries, and cluster binding energies for Si_8.

Wave function	State	Total energy (hartree)	Bond length (Å)		Bond angle (deg)		Binding energy (eV/atom)
HF-ECP	$^1A_1$	−2311.072 629	Si(1)—Si(2)	2.26	Si(1)-Si(5)-Si(3)	66.9	1.48
			Si(1)—Si(3)	2.67	Si(5)-Si(1)-Si(2)	110.9	
D_{2d} TBN cluster			Si(1)—Si(5)	2.42	Si(5)-Si(1)-Si(6)	110.7	
HF-ECP	$^1A_{1g}$	−2311.091 106	Si(1)—Si(2)	2.51	Si(1)-Si(3)-Si(2)	54.1	1.55
			Si(1)—Si(3)	2.71	Si(3)-Si(1)-Si(4)	52.9	
D_{6h} PBN cluster			Si(3)—Si(4)	2.40	Si(3)-Si(4)-Si(1)	63.6	
					Si(3)-Si(4)-Si(5)	120.0	
HF-ECP	^1A_g	−2311.163 653	Si(1)—Si(2)	2.34	Si(1)-Si(2)-Si(4)	117.9	1.79
			Si(1)—Si(8)	2.60	Si(2)-Si(1)-Si(3)	64.3	
C_{2h} PBN cluster			Si(2)—Si(3)	2.49	Si(2)-Si(4)-Si(3)	59.5	
			Si(2)—Si(4)	2.50	Si(2)-Si(4)-Si(5)	108.0	
			Si(2)—Si(6)	2.53	Si(2)-Si(6)-Si(5)	116.2	
			Si(4)—Si(6)	2.79	Si(2)-Si(6)-Si(8)	67.2	
					Si(4)-Si(5)-Si(6)	68.4	
GVB-ECP	^1A_g	−2311.289 020	HF geometry				1.84
HF-ECP	^1A_g	−2311.116 826	Si(1)—Si(2)	2.38	Si(1)-Si(2)-Si(4)	100.9	1.64
			Si(2)—Si(3)	2.65	Si(1)-Si(2)-Si(6)	108.0	
D_{2h} TBN cluster			Si(2)—Si(6)	2.44	Si(2)-Si(1)-Si(3)	67.7	
					Si(2)-Si(3)-Si(7)	90.0	
GVB-ECP	^1A_g	−2311.292 142	HF geometry				1.86

This structure therefore resembles two layers of atoms in a hexagonal close-packed arrangement.

We also optimized two other structures for Si_8 that are shown schematically in Figs. 12(b) and 12(c). Figure 12(b) shows a TBN cluster that consists of four five-membered rings and resembles a fragment from the π-bonded chain model for the (2×1) reconstructed Si(111) surface.[46] The total energy and geometry for that structure are given in Table VII; the structure was 0.70-eV above the D_{2h} tetrahedral structure at the HF level. Figure 12(c) shows a PBN cluster that is a bicapped hexagon. This cluster is a natural continuation of the sequence of cluster structures with 5–7 atoms, where two-center–two-electron bonds are sequentially replaced by three-center–two-electron bonds (interstitial pairs). However, geometrical constraints in bond lengths in the eight-atom cluster destabilize it considerably. In order to have physically reasonable bond lengths between atoms in the horizontal mirror plane, the bond lengths between those atoms and the atoms on the rotation axis [Si(1) and Si(2)] become elongated so that the cluster is destabilized. The HF-ECP binding energies for the series (D_{3h}) Si_5, (C_{2v}) Si_6, (D_{5h}) Si_7, and (D_{6h}) Si_8 are: 1.73, 1.85, 1.95, and 1.35-eV/atom, respectively—falling considerably when a sixth atom is added in the horizontal mirror plane. The HF-ECP equilibrium bond distances for D_{6h} Si_8 are the following: 2.40 Å between atoms in the plane; 2.71 Å between atoms in the plane and atoms on the axis, and 2.51 Å for the long-bond distance.

G. Si_{10}

Two PBN clusters have previously been proposed[18,20,24] as equilibrium structures for Si_{10}. These are a tetracapped octahedron (T_d) and a C_{3v} structure that is related to the T_d structure by rotating a capping atom and the three atoms bonded to it [Si(1)-Si(5)-Si(6) and Si(7) in Fig. 16(a)] by 30° about the threefold rotation axis through Si(1). We have performed HF and GVB calculations on the T_d structure taken from Ref. 18 and on the TBN cluster with D_{2h} symmetry shown in Fig. 15. The geometry of the TBN structure (Table VIII) was estimated by taking geometrical parameters from the equilibrium geometries of D_{2d} Si_6 (Fig. 7) and D_{2h} Si_8 (Fig. 13). Thus neither of these structures was optimized using the ECP basis set in which the calculations were performed, but we do not expect this to affect our conclusions qualitatively. At the geometries chosen, the T_d PBN cluster was 2.62-eV below the D_{2h} TBN cluster at the HF level; at the GVB level this energetic difference was reduced to less than 0.01 eV. Again there are important correlation effects in the four long bonds of the TBN cluster neglected by the HF wave function, while there are no long bonds (or other pairs with energetically important correlation effects) in the PBN cluster. The D_{2h} cluster is considerably more stable than a fragment of the diamond lattice resembling the hydrocarbon adamantine that has been optimized previously.[18,20] The latter contains 12 bent bonds, 6 lone pairs, and 4 high-spin dangling orbitals coupled into an overall quintet state;[18] the D_{2h} TBN cluster contains 14 bent bonds, 4 long bonds, and 2 lone pairs, giving it *six* more bonding pairs than the adamantine structure. The D_{2h} structure is shown schematically in Fig. 15(a). Contour plots of the four unique bond pairs of the cluster are shown in Figs. 15(c)–15(f). Note the transferability of GVB orbitals (c)–(e) between Si_8 (Fig. 13) and Si_{10} D_{2h} structures.

A schematic representation of the PBN cluster is

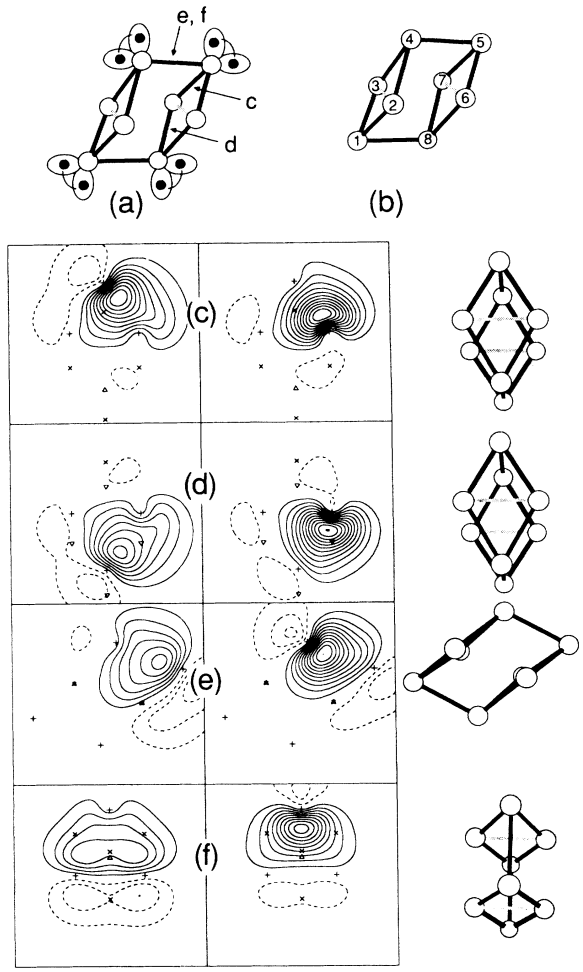

FIG. 14. (a) Schematic diagram and (b) molecular structure of PBN C_{2h} ^1A_g Si_8; (c) orbitals forming the Si(5)—Si(7) bent bond; (d) orbitals forming the Si(7)—Si(8) bent bond; (e) orbitals forming the Si(4)-Si(5)-Si(6)-Si(7) interstitial pair; (f) the same pair in a plane containing atoms Si(4), Si(6), and Si(7) showing the interstitial δ character of the pair.

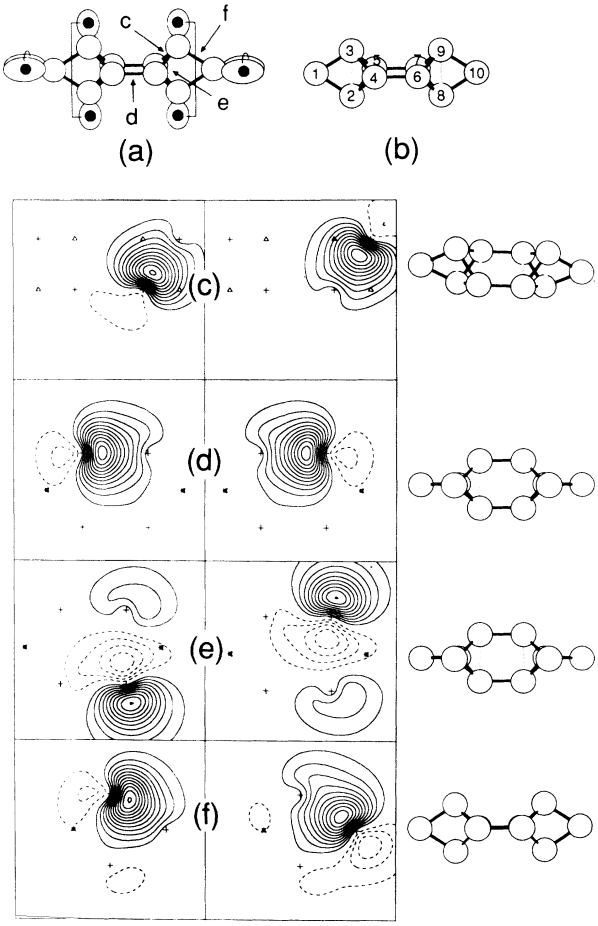

FIG. 15. (a) Schematic diagram and (b) molecular structure of TBN D_{2h} ^1A_g Si_{10}; (c) orbitals forming the Si(6)—Si(9) bent bond; (d) orbitals forming the Si(5)—Si(7) bent bond; (e) orbitals forming the Si(6)—Si(7) long bond; (f) orbitals forming the Si(9)—Si(10) bent bond.

TABLE VIII. Total energies, equilibrium geometries and cluster binding energies for S_{10}.

Wave function	State	Total energy (hartree)	Bond length (Å)		Bond angle (deg)		Binding energy (eV/atom)
HF-ECP	^1A_g	−2888.928 787	Si(1)—Si(2)	2.45	Si(1)-Si(2)-Si(4)	97.7	1.72
			Si(2)—Si(3)	2.74	Si(2)-Si(1)-Si(3)	68.0	
D_{2h} TBN cluster			Si(2)—Si(4)	2.34	Si(2)-Si(4)-Si(3)	71.7	
			Si(4)—Si(5)	2.74	Si(3)-Si(4)-Si(6)	124.1	
			Si(4)—Si(6)	2.44	Si(4)-Si(3)-Si(5)	71.7	
					Si(5)-Si(4)-Si(6)	90.0	
GVB-ECP	^1A_g	−2889.157 388	HF geometry				1.97
HF-ECP	$^1A_1$	−2889.025 102	Si(1)—Si(5)	2.38	Si(1)-Si(5)-Si(6)	57.3	1.99
			Si(5)—Si(6)	2.57	Si(5)-Si(1)-Si(6)	65.3	
T_d PBN cluster					Si(5)-Si(6)-Si(7)	60.0	
					Si(5)-Si(7)-Si(10)	60.0	
GVB-ECP	$^1A_1$	−2889.157 722	HF geometry				1.97

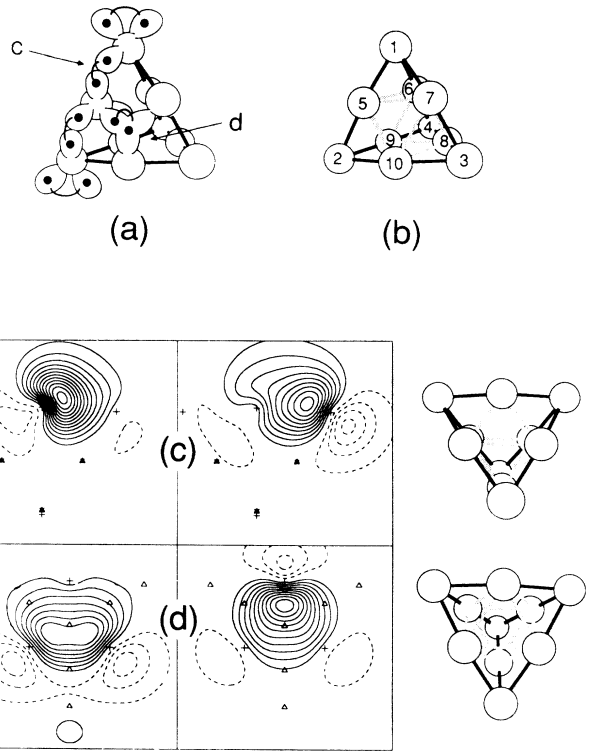

FIG. 16. (a) Schematic diagram and (b) molecular structure of PBN T_d $^1A_1$ Si_{10}; (c) orbitals forming the Si(1)—Si(5) bent-bond pair; (d) orbitals forming the Si(5)-Si(7)-Si(10) interstitial pair.

shown in Fig. 16(a). Each capping atom [Si(1)—Si(4)] is bonded to three atoms of the octahedron by three bent bonds and each of these atoms also has an angularly correlated lone pair giving those atoms five localized orbitals. The remaining four faces of the octahedron have interstitial pairs localized in them. There are therefore four atomiclike orbitals on each of the atoms in the octahedron [Fig. 16(a)]: two orbitals on each atom participate in bent bonds to capping atoms and two contribute to interstitial pairs. Contour plots of GVB orbitals representing one of the bent bonds and one of the interstitial pairs are shown in Figs. 16(c) and 16(d), respectively. This structure may also be regarded as three layers of an fcc lattice because of the *ABC* stacking sequence of the horizontal layers in Fig. 16(b). Regarded in that way, the C_{3v} structure[18,24] consists of three layers in an hcp stacking sequence (*ABA*), capped by a single atom.

IV. PREDICTED STRUCTURES FOR CLUSTERS WITH 20–50 ATOMS

Reactivities of clusters in the size range ~5–60 atoms towards three kinds of reagent have been studied experimentally. The relative reactivity of a particular cluster towards a particular reagent, compared to that of other clusters of neighboring size, depends on the class of reagent being used so there are no *universal* cluster magic numbers, i.e., not all clusters that display a low reactivity towards a particular reagent will also be relatively unreactive towards other reagents. This reaction behavior is still not well-understood but we may classify the reagents used so far according to the type of reaction observed: (1) those that chemisorb associatively (e.g., ethylene);[47] (2) those that chemisorb dissociatively (e.g., ammonia, methanol);[6,48] (3) those that promote etching reactions (e.g., oxygen, nitrogen dioxide).[4,47] Larger clusters with more than 20 atoms are known to adsorb several ethylene molecules without fragmenting.[47] Reagents that undergo dissociative chemisorption have reactivities that depend on the cluster size and there is a series of magic-number clusters that are particularly unreactive.[5] Etching reagents remove one or two SiO molecules from the parent cluster.[4,6,47] An experimental observation from reaction kinetics studies that further complicates matters is that for many clusters there are actually two isomers present in the beam that have dramatically different reactivities.[47,48] It is possible, therefore, that clusters with interstitial pair bonding and tetrahedral orbital bonding are both experimentally isolatable even up to 30 or more atoms.

In the preceding section we showed that a substantial fraction of the valence electron pairs in both TBN and PBN clusters were nonbonding lone pairs. In this section we propose structures for TBN clusters with no lone pairs and only four nonbonding unpaired electrons in clusters with more than 20 atoms. Having considered the size at which clusters might revert to a bulklike bonding scheme, i.e., an extended tetrahedral-bonding network, we postulate that the increase in stability of a TBN cluster, when it can be formed without lone pairs, is sufficient to increase the stability of TBN clusters over that of PBN clusters so that PBN clusters are metastable and will not be observed experimentally in large clusters. We show that a series of TBN clusters can account for experimental data on reactivities of positive cluster ions with 20–50 atoms towards ammonia or methanol. These clusters are judged to be stable because their structures are not highly strained, they have no long pairs and contain structural features already observed in reconstructed silicon surfaces; since they also account for the experimental reactivity data, we suggest that the equilibrium structures for clusters with more than 20 atoms are based on tetrahedrally bonded cores, and clusters with "magic numbers" of atoms contain the correct number to form a "defect-free" cluster that is less reactive towards dissociatively chemisorbing reagents than clusters with a few atoms more or less than the "magic-number" cluster. Clusters with these proposed structures ought to adsorb several ethylene molecules since they possess dimer bonds that have orbitals appropriately oriented for ethylene chemisorption.

What size of core is necessary for such a cluster? Extending out from a central atom in the cubic diamond lattice the number of atoms in a "shell" is 1, 4, 12, 36, . . . , with core size of 1, 5, 17, 53, . . . , atoms. A TBN cluster must contain a *core* of at least 17 atoms in order to be completed without any lone pairs or large numbers of dangling orbitals; those 17 atoms consist of a central

atom and a first and second shell of tetrahedrally bonded atoms.

Lifetimes of positive cluster ions exposed to ammonia or methanol while held in a cyclotron orbit show that they have dramatic oscillations in reactivity depending on the number of atoms in the cluster ion; there are 2 orders of magnitude difference in reactivity between the most (Si_{43}^+) and least reactive (Si_{39}^+) clusters.[5] Minima in a curve of reactivity versus number of atoms occur at 21 atoms,[49] and at 25, 33, 39, and 45 atoms;[5] these are the cluster magic numbers. Further interesting features of clusters in this size range are the following: a smooth variation in the amount of each cluster produced in the beam—none of the clusters is formed in much greater abundance than its neighbors, unlike the situation in similar experiments with carbon clusters;[50] rapid oscillations in reactivity with cluster size cease for clusters with more than 47 atoms.[5]

The authors of the experimental work have suggested that the oscillations in reactivity may by explained in terms of cluster structure and that clusters of this size could have a stable core of at least five tetrahedrally bonded atoms.[5] We have investigated what these structures might be by considering all the possible structures for a 17 atom core and high- and low-symmetry means of completing the structures. We find that there are only two plausible 17-atom cores that give rise to two series of clusters that account for the "magic numbers" above; clusters with these numbers of atoms form symmetric structures that are "defect free" and therefore should exhibit a lower reactivity than their neighbors. The two types of core are similar in that the bonds joining the first and second shells of atoms are staggered with respect to the bonds joining the central atom and the first shell (as in bulk diamond structure silicon); alternatively, if these two sets of bonds are eclipsed the resulting structure is very open and is impossible to complete without a large number of dangling orbitals. The types of core are distinguished by the orientation of the dangling orbitals of the second shell of atoms; if the orbitals eclipse the bonds joining the central atom to the first shell then a structure is formed which may be tetracapped, as shown in Fig. 17(a). If the orbitals in the second shell are rotated from this position by 60° so that they eclipse the bonds joining the first and second shells, capping atoms may be bonded in sites resembling T_4 adatom sites on the Si(111) surface [Fig. 17(b)]; for this reason, clusters with this core are referred to as T_4 clusters, while clusters containing the previous kind of core are referred to as H_3 site in models of silicon surfaces. Cluster cores where some of the dangling orbitals are rotated in one fashion and some in the alternative fashion *cannot be completed without many dangling bonds.*

Both capped cluster cores have tetrahedral symmetry and possess six rectangular arrangements of four dangling orbitals; one set of these dangling orbitals is labeled $A-D$ in Fig. 17 (a) and one is labeled $S-V$ in Fig. 17(b). These dangling orbitals pair up to form bonds in the 21 atom cluster or participate in bonds to dimers, trimers, or tetramers (Fig. 18) of atoms in the larger clusters. Subtracting the tetracapped cores from the "magic-number" clusters[49] leaves 0, 4, 12, 18, and 24 atoms to complete the clusters. Since there are six equivalent sites each with four dangling orbitals in a rectangular arrangement, there are either no atoms, two dimers, six dimers, six trimers, or six tetramers required to complete the cores in the "magic-number" clusters. Structures of the clusters are now considered individually.

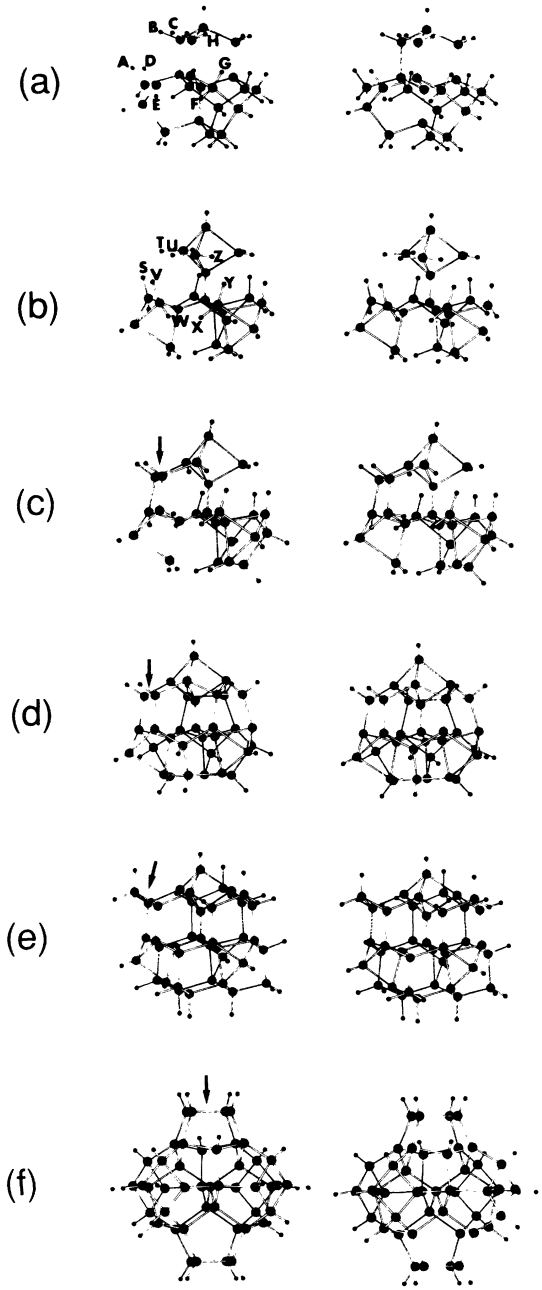

FIG. 17. Stereographic pairs of proposed structures for magic-number clusters. Atoms are indicated by larger circles and dangling electrons (which are spin paired when they occur in dimers, trimers, or tetramers) are indicated by smaller circles. (a) H_3 Si_{21} (the uppermost atom is a capping atom and there are three additional, equivalent atoms); (b) T_4 Si_{21} (the uppermost atom is a capping atom and there are three additional, equivalent atoms); (c) T_4 Si_{25}; (d) T_4 Si_{33}; (e) T_4 Si_{39}; (f) H_3 Si_{45}.

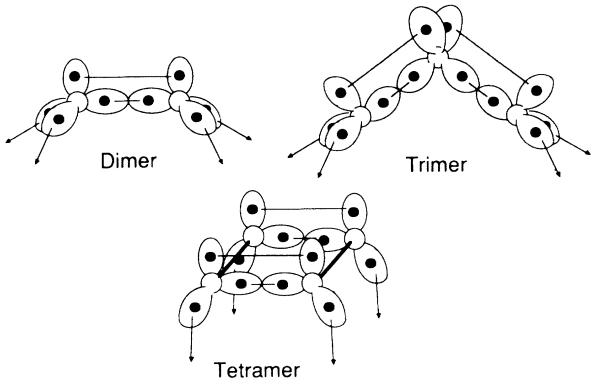

FIG. 18. Bonding configurations in proposed "terminating clusters" of larger TBN clusters. Arrows indicate covalent bonds to the H_3 or T_4 cluster cores.

A. Si_{21}

Inspection of the stereographic pairs of the cluster cores in Figs. 17(a) and 17(b) shows that pairs of dangling orbitals around a threefold axis in the T_4 cluster [$U-Z$ in Fig. 17(b)] are appropriately oriented to overlap and form bonds; there are four such axes so the dangling orbitals of the cluster core (with the exception of the dangling orbitals on the four capping atoms) can be saturated without adding any atoms and the structure has four three-membered rings. [The possibility of forming such a 21 atom cluster is readily confirmed by constructing a three-dimensional (3D) model using atoms with tetrahedral lobes.] On the other hand, dangling orbitals in the H_3 cluster core [$C-H$ in Fig. 17(a)] are oriented in ways that allow minimal overlap so it is not favorable to form a stable H_3 cluster with 21 atoms. In fact dangling orbitals in one of the six equivalent rectangular arrangements of dangling orbitals of the H_3 cluster core [$A-D$ in Fig. 17(a)] are nearly parallel to one another, whereas they point more directly towards each other [$S-V$ in Fig. 17(b)] in the T_4 cluster core. The H_3 core is therefore more appropriate for larger clusters in which, for example, tetramers complete the core, i.e., Si_{45}, while the T_4 core is more suited to smaller clusters that require no atoms, dimers, or trimers for completion. Thus the T_4 core, whose dangling orbitals are saturated by pairing-up internally, is the proposed structure for Si_{21}.

B. Si_{25}

Si_{25} is formed by adding two dimers to Si_{21} on opposite sides of the cluster. The dimer structure, similar to the dimer structure in the (2×1) reconstruction of the Si(100) surface,[51] is shown in Fig. 18. By breaking bonds in the three-membered rings of Si_{21}, 1–6 dimers can be added yielding clusters with 23, 25, 27, 29, 31, and 33 atoms; with the exception of Si_{23}, none of these clusters was highly reactive, but the cluster with the minimum reactivity was Si_{25}. Why should Si_{25} be particularly unreactive? There are two mechanisms that relieve strain in this cluster, compared to Si_{21}, which we expect to contribute to its relative inertness towards ammonia or methanol. When two dimers are added on opposite sides of Si_{21} all of the three-membered rings are converted to four-membered rings *and* this cluster is able to distort from T_d symmetry to C_{2v} symmetry enabling strain in the 21 atom core to be relieved also. Adding more dimers does not give such a large reduction in the strain of the cluster and so no dramatic reductions in reactivity are expected. The added dimers in Si_{25} are illustrated in Fig. 17(c); one of these is labeled by an arrow. The next significant stabilization occurs when a maximum of six dimers has been added because then all three-membered rings in Si_{21} are converted to six-membered rings.

C. Si_{33}

Adding six dimers to the T_4 Si_{21} cluster core by breaking all the bonds in the three-membered rings yields Si_{33}. It has four six-membered rings in place of the three-membered rings in Si_{21} and it possesses full T_d symmetry. the structure is shown in Fig. 17(d); one of the six dimers is labeled by an arrow. The surface of this cluster contains adatom and dimer pairs exactly like those in the (7×7) reconstruction of the Si(111) surface except that the dimers are π bonded in the cluster, whereas those orbitals used to form π bonds in the cluster form bonds to other atoms in the reconstructed surface. The "π bonds" in these clusters as well as those invoked in the literature of silicon surfaces are not strictly of π symmetry, but we refer to them as such to be consistent with the existing nomenclature of the literature. We used a Keating-type potential[52] to suggest geometries for clusters with 33, 39, and 45 atoms. There are no highly strained or unusual bonds in any of these clusters and it is not surprising to find that the 39 and 45 atom cluster ions had the lowest reactivity in the range of cluster sizes studied.[5] A more quantitative approach to the structures and total energies of all of these clusters (with T_4 or H_3 cores) using a classical potential based on valence-bond methods is being pursued.[53]

D. Si_{39}

The replacement of all dimers in Si_{33} by trimers is effected by inserting an atom into each dimer bond; this results in our proposed structure for Si_{39}. This structure is actually a tetracapped, 35-atom, three-layer slab of the bulk silicon structure. It is therefore expected to be very stable. Bonding in the trimer is expected to take the form shown in Fig. 18, i.e., each trimer has two single bonds and two twisted π bonds that resemble the π-bonded chain of the (2×1) reconstruction of the Si(111) surface.[46] The only dangling orbitals of the cluster are those on the four adatoms. The structure of Si_{39} is shown in Fig. 17(e) with a T_4 core of atoms (one of the six trimers is labeled by an arrow). It is not clear, however, whether this is the most stable cluster, or whether a similar cluster in which an H_3 core completed by trimers, is more stable. However, when 3D models of the structures are constructed, the dangling orbitals of the T_4 core form bonds to trimers with less strain; this point will be tested using classical force fields for the cluster.[53]

E. Si_{45}

The outwardly oriented dangling orbitals in the H_3-cluster core are ideally suited to form bonds to tretramers as shown in Fig. 18. Stereographic pairs of the Si_{45} cluster are shown in Fig. 17(f); one of the tetramers is labeled by an arrow. Each tetramer contains two π bonds and distorts into a rectangle to form bonds to the core with a minimum of strain using a Keating-type potential. In contrast to the 39-atom cluster, it is easy to decide which core is more stable for this cluster size; if tetramers are bonded to the T_4 core there are four nine-membered rings on the surface that are highly strained and exclude the T_4 cluster as a possible equilibrium structure for Si_{45}. The H_3 cluster exterior consists exclusively of five-membered rings except for the rectangular dimers, while the interior consists of six-membered rings. There are 76 single bonds, 12 π bonds and four dangling orbitals in this cluster. This contrasts with a structure[54] for the 45-atom cluster that is terminated exclusively by atoms with dangling orbitals that are postulated to form a 2D equivalent of a π-bonded chain; in this latter structure[54] there are 70 single bonds and 20 π bonds and the surface contains five-, six-, and seven-membered rings. Whether either of these structures corresponds to the actual structure of Si_{45} can only be decided by further calculations and experimental work.

In summary, clusters with 21, 25, 33, and 39 atoms are proposed to have T_4 cluster cores [Fig. 17(b)] and are completed by internal bonds, dimers, or trimers, while the 45-atom cluster has an H_3 core [Fig. 17(a)] and is completed by tetramers. Large changes in stability at these magic numbers, compared to clusters with a few atoms more or less, are provided by the following: saturation through internal bonding (Si_{21}), relief of strain by changing all three-membered rings to four-membered rings and distortion to lower symmetry (Si_{25}), extension of all rings to six-membered rings (Si_{33}), extension of all dimers to trimers, yielding a tetracapped, bulklike structure (Si_{39}), and capping all dangling orbitals with tetramers (Si_{45}). These changes in stability compared to their neighbors result in minima in a curve of reactivity versus the number of atoms in the cluster. All of the clusters proposed have quintet electronic spin states. Finally, it is impossible to construct a low-energy structure that contains more than 45 atoms around a 17 atom core; clusters with more than 45 atoms must begin to have cores larger than the H_3 or T_4 cores. Clusters with larger cores may require very large numbers of atoms (>100, say) before any clusters without surface defects are possible and these have not been studied experimentally. Therefore it is easy to explain why the observed oscillations in reactivity cease above 47 atoms[5]—there are no more "magic-number" clusters until considerably larger cluster sizes are reached.

V. DISCUSSION

In this section we briefly summarize results described above and note the analogies between the geometric and electronic structures of the clusters and the corresponding properties of the Si(111) (7×7) reconstructed surface. Although less direct, there are also some analogies between PBN clusters and the high-pressure phases of silicon. We do not believe these analogies to be fortuitous, but rather the result of the underlying similarities in *local electronic structure.*

We have shown that there are two kinds of silicon cluster in the size range studied. They are classified according to their bonding characteristics that we have called tetrahedral- and polyhedral-bonding networks. TBN clusters have fairly open structures (although not as open as fragments of the cubic diamond lattice) and there are ~ 3 electron pairs around each atom making them formally electron deficient. TBN clusters are characterized by possessing exclusively two-center electron-pair bonds and lone pairs. There are two kinds of electron-pair bonds in the TBN clusters, namely bent bonds, and long bonds. Of the three kinds of electron pairs, lone pairs are shown to contribute least to the stability of a cluster; hence, clusters with more lone pairs are less stable. The average bent-bond length in tetrahedral clusters is 2.43 Å, ranging from 2.36–2.50 Å in the most stable TBN cluster of each size. The average long-bond length is 2.77 Å, ranging from 2.67–2.81 Å.

PBN clusters are more compact than TBN clusters. In the most compact clusters (such as T_d Si_{10}) many of the atoms are surrounded by four electron pairs. There are also four electron pairs about some of the atoms in less compact clusters (such as the ground state of Si_6). This feature makes the PBN clusters less electron deficient than the TBN clusters. In addition to the bent bonds, long bonds, and lone pairs found in TBN clusters, the PBN clusters are characterized by having interstitial electron pairs localized in triangular faces or tetrahedral interstices. The average bent-bond distance in PBN clusters is 2.43 Å (the same as TBN clusters) with a range of 2.34–2.60 Å, while the average long-bond distance is 2.66 Å (somewhat shorter than in TBN clusters) with a range of 2.49–2.73 Å. The average interatomic distance between atoms bonded by an interstitial pair is 2.51 Å with a range of 2.46–2.57 Å. The compactness of the PBN clusters does not arise because of shorter bond distances but through more efficient packing of the atoms. The more efficient packing of atoms is, in turn, a consequence of the formation of *interstitial* (or *multicenter*) *bonds*, which allows a more efficient sharing of electron pairs.

Valence electron pairs in TBN clusters have been shown above to be localized exclusively in bent bonds, long bonds, and lone pairs. Covalent bonding schemes for diamond lattices of group-IV elemental solids (C, Si, Ge) have been familar in the solid-state physics literature for many years and covalent bonding models can also be proposed for reconstructed silicon surfaces in which there are (exclusively) bent bonds and dangling bonds in the Si(111) (7×7)-reconstructed surface and, additionally, "π bonds" in the Si(111) (2×1)- and Si(100) (2×1)-reconstructed surfaces. There have been significant advances in knowledge of the structures of reconstructed silicon and germanium surfaces in the past five years since the dimer adatom and stacking fault (DAS) atomic arrangement of the (7×7) reconstruction of Si(111) was

determined by TEM diffraction[55] and we make direct comparisons between the atomic arrangement of two TBN clusters and that surface. More recently, x-ray scattering,[56] reflection high-energy electron diffraction (RHEED),[57] and LEED,[58] experiments have provided accurate structural parameters for that surface. Structures have also been determined for reconstructed surfaces containing ordered group-III,[59] -IV,[60] or -V,[61] impurity adatoms.

Some general observations may be made on this body of information. First, for either silicon or germanium (111) surfaces, clean or containing impurity atoms, there are usually several ordered structures to be found in a microscopic region of a surface that has undergone the same treatment. Scanning-tunneling microscope (STM) measurements on Si(111) on a region $\sim 100 \times 100$ Å^2 have shown structure with (9×9), (7×7), (5×5), ($\sqrt{3} \times \sqrt{3}$), and (2×2) periodicities.[62] Second, transitions between one periodicity and another may be effected by laterally straining the reconstructed surface by growing several layers of the solid on a substrate with a slight lattice mismatch[60,63] or by adsorbing impurity atoms that substitute for Si or Ge adatoms.[59,60] Third, all reconstructions mentioned above are comprised of some or all of the local-bonding arrangements that are referred to as dimers, adatoms, rest atoms (which are surface atoms with three bent bonds and a dangling bond but no atom directly beneath, which distinguishes them from adatoms), and stacking faults. The DAS structure of Si(111) (7×7) contains all of the above and the structure of the Ge(111) $c(2\times8)$ surface has now been shown to consist of adatoms and rest atoms.[64] A principal concern has been the role of strain[65] in the reconstructed layers because, although the structures of the Si and Ge reconstructed (111) surfaces have tetrahedral-bonding networks, there are significant deviations from the diamond-structure bulk-crystal bond-length values that are 2.35 and 2.44 Å for Si and Ge, respectively. Since different reconstructions are produced by minor changes in the chemical composition of the surface, surface treatment, or applied stress, different surface structures are viewed as having small differences in total energy and strain is important in determining which structure is energetically preferred.

The problem of understanding strain in these surfaces may be simplified by considering them to consist of discrete five-atom units (when no dimers are present; see Fig. 3) or seven-atom units [Fig. 1(c)], which are bonded to one another (parallel to the surface) and to the surface itself. Internal stress in these units cancels at their equilibrium geometries, so a measure of the strain caused by bonding them to each other or the surface (external strain) may be obtained by comparing the structure of the isolated cluster and the equivalent unit of atoms embedded in the surface. From this viewpoint, the equilibrium geometries of five- and seven-atom clusters are better reference geometries when strain is being compared in different systems than the bulk-diamond-structure bond distances and the tetrahedral angle. We compare bond lengths and angles in Si_5 and Si_7 TBN clusters to those in the (7×7)-reconstructed Si(111) surface determined by LEED (Ref. 58) in Fig. 19. There is good agreement between the LEED structure and the structure obtained by combining parallel and perpendicular structural parameters from RHEED (Ref. 56) and x-ray scattering,[57] and with a semiempirical total-energy minimization calculation.[66] The DAS (7×7) unit cell of Si(111) can be entirely constructed from these seven-atom units (with the exception of six TBN rest atoms per unit cell); these units are also an important feature of the structure we have proposed for Si_{33}. The current model for the structure of the Ge(111) $c(2\times8)$ surface consists of ordered adatoms and rest atoms and can therefore be entirely constructed from embedded five-atom units with four additional TBN rest atoms per unit cell. The five- and seven-atom TBN clusters are therefore of considerable importance even though the relevant Si_7 TBN cluster [Fig. 1(c)] is not the ground-state structure of Si_7.

The seven-atom cluster is bonded to the surface [Figs. 19(b) and 19(c)] *via* orbitals labeled "*a*." Two of these are angularly correlated lone-pair orbitals in the gas-phase cluster and one is part of a long bond. In the reconstructed surface these lone-pair and long-bond orbitals are recoupled leaving two hybrids "*b*" to form bonds to atoms in another equivalent unit and a dangling orbital "*c*" on the adatom that is shown as being weakly singlet coupled to another equivalent orbital in Fig. 19(c). The remaining lone pair "*d*" is used to form two bonds to atoms surrounding a rest atom. Three observations can be made: (i) all except one of the bond distances in the

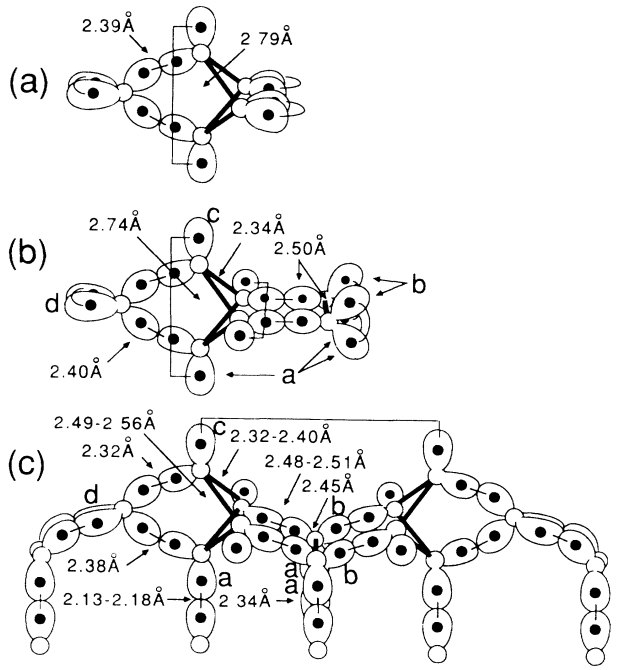

FIG. 19. Bond lengths and tetrahedral hybrids in (a) TBN D_{3h} Si_5 cluster; (b) TBN C_{2v} Si_7 cluster; (c) ranges of bond lengths determined by LEED in the Si(111) (7×7)-reconstructed surface. Experimental bond lengths are from Ref. 58.

cluster are within the range of experimentally determined distances in the reconstructed surface [a range of bond distances is indicated in Fig. 19(c) because the seven-atom units occur in several different environments in the unit cell, i.e., in faulted or unfaulted halves of the (7×7) unit cell, etc.]; (ii) the dimer bond and the bonds to the dimer parallel to the surface (partly comprised of "*b*" orbitals) are significantly longer than the bulk bond distance without any *external* strain—they were both determined to be 2.50 Å in the cluster, while the dimer bond in the surface is 2.45 Å and bonds to the dimer are between 2.48 and 2.51 Å; (iii) the separation of the surface adatom from the atom directly beneath it is much less than the typical long-bond distance in clusters -2.74 Å for Si_7.

Hence, according to this analysis, the dimer in the surface is actually in slight compression and the bonds to the dimer are around their natural length, so we conclude that this part of the surface structure is determined by internal strain in the cluster and not external strain involved in bonding the cluster to the surface. The chief difference in adatom bonding situations in the Si_7 cluster and in the surface is the existence, or not, of a long bond to the adatom. When the long bond, with one orbital labeled "*c*" in Fig. 19(b), is removed and its constitutent orbitals are recoupled with other surface orbitals [Fig. 19(c)], Pauli repulsions between the long bond and bent bonds, present only in the isolated cluster, are absent. This permits the adatom to relax into the surface; the difference between equivalent interatomic distances in the cluster and the surface is 0.22 Å. The driving force for this relaxation is increased overlap of orbitals forming bent bonds to the adatoms. Evidence for this is that the average (calculated) length of bent bonds around long bonds in the clusters is longer than bent bonds to the surface adatom.

Before considering the analogies between clusters and bulk silicon, we note that silicon undergoes a series of phase transitions as a function of pressure at ambient temperature in which the atomic volume steadily decreases and the coordination number increases; the equilibrium phases at the highest pressures are close-packed structures. There are six phases whose structures are well established experimentally and there is good agreement in general between experiment[67–72] and the results of pseudopotential local-density total-energy calculations[73–77] on phase stability as a function of pressure. All of the high-pressure phases are metallic. In each of the close-packed phases the valence charge density is (necessarily) located in interstitial regions and this is revealed by charge-density plots from the total-energy calculations.[75,77]

We now compare the PBN Si_8 (C_{2h}) and Si_{10} (T_d and C_{3v}) clusters with the close-packed lattices (fcc and hcp) and observe the similarities and differences in their electronic structures. In Fig. 20 an fcc cell and the relationship to the approximate structures of the PBN Si_8 and Si_{10} clusters are shown. The fcc cell contains eight tetrahedral interstices (outlined by shaded lines in the figure) and four octahedral interstices (one of these is outlined by solid lines and there are a further twelve $\frac{1}{4}$ octahedral interstices that are shared with adjacent cells). A

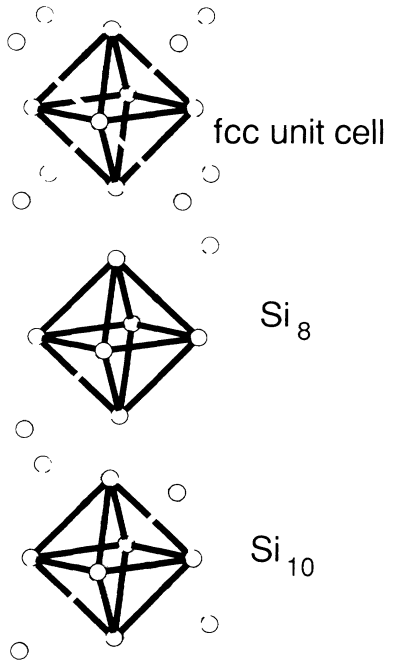

FIG. 20. A comparison of structures of an fcc cell and PBN Si_8 and Si_{10} clusters. The octahedral interstitial site enclosed in the unit cell is outlined by solid lines and the tetrahedral sites are outlined by shaded lines.

C_{3v} Si_{10} structure originally reported by Ballone[24] and geometry optimized by Raghavachari[18] may be regarded as a monocapped hcp structure with three, three-atom layers. The *local structural relationships* between the clusters and the high-pressure solid phases are clear but these structural similarities are not entirely reflected in the electronic structures.

A calculated valence charge density for bulk fcc silicon in the (100) plane is redrawn from Ref. 77 in Fig. 21. There is clearly a charge buildup in the tetrahedral interstices of the solid and charge depletion in the octahedral interstices (the location of these sites was given in Fig. 20). Since there are eight valence electron pairs per fcc cell (as it is shown in Fig. 20) it is possible to occupy (on average) each tetrahedral site with one electron pair. As noted earlier when the bonding in C_{2h} Si_8 was described, there are two electron pairs in that cluster that occupy quite localized orbitals in tetrahedral interstitial sites, thus exhibiting a parallel between the electronic structure of the fcc solid and PBN Si_8. However, most of the orbitals in PBN clusters are not involved in interstitial bonds, they are involved in two-center two-electron bonds, and low-lying excitations will clearly be quite different than in metallic silicon. Hence, it is quite understandable that voltage-dependent scanning-tunneling microscope studies have shown that Si_{10} clusters adsorbed on a clean gold surface have a band gap of ~1 eV,[78] which contrasts with the metallic properties of the solid phases.

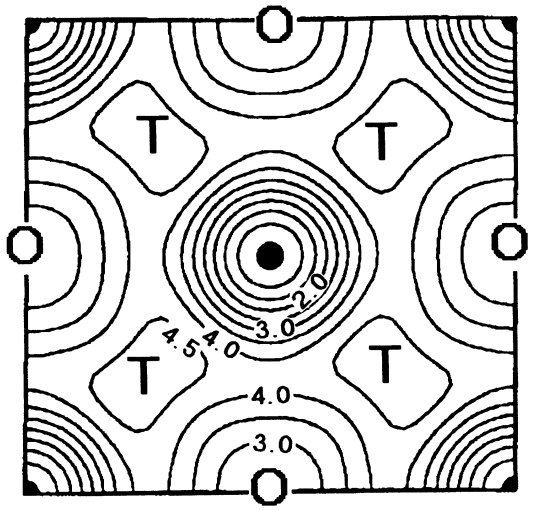

FIG. 21. Calculated valence charge density of fcc silicon in the (100) plane reproduced from Ref. 77. The units are in electrons per unit cell, hence 4.0 is the average density. The charge density reaches its maximum value of 4.76 electrons per unit cell in the tetrahedral interstitial sites labeled "*T*." Octahedral interstitial sites, which are depleted of charge density, are labeled "*O*." There are additional, unlabeled octahedral interstitial sites above and below the atom at the center of the diagram.

VI. SUMMARY AND CONCLUSIONS

We have presented the first valence-bond treatment of silicon clusters and the first in-depth analysis of their bonding. The *ab initio* generalized-valence-bond (GVB) method was employed to compute the electronic structure and bonding. From the calculations, two classes of silicon cluster have been identified: (1) TBN clusters possessing *bent bonds, long bonds,* and *lone pairs* have structures and bonding similar to fragments of the Si(111) (7×7)-reconstructed surface; (2) PBN clusters possess *interstitial bonds* in addition to the kinds of electron pair in TBN clusters. The stability of the PBN clusters stems from increased electron-nuclear attraction compared to TBN clusters. Qualitatively this is the result of the more effective distribution of electron pairs in PBN clusters that have interstitial bonds.

However, in two cases (Si_8 and Si_{10}) the most stable TBN and PBN clusters have almost identical energies according to the GVB results (thus, both structures might be observed experimentally). TBN clusters larger than Si_5 possess more long bonds than in PBN clusters of the same size. As the long bonds have considerably greater intrapair-correlation energies than the other kinds of bonds mentioned, the (uncorrelated) HF method is sometimes biased against the TBN clusters, because of their long bonds, to such an extent that a qualitatively different result is obtained. The GVB results presented here are the first to explicitly include the important intrapair-correlation effects for silicon clusters.

Many of the features found in the smaller clusters are likely to be absent in larger clusters where a bulklike core of 17 atoms is postulated to occur. We have proposed a series of structures with such cores for clusters with 21, 25, 33, 39, and 45 atoms, which we postulate to be the most stable structures for those cluster sizes. In those structures the dangling orbitals of two alternative TBN 17-atom cores are terminated by dimers, trimers, or tetramers of atoms and their surface structures are similar to the Si(100) (2×1) and Si(111) (2×1) reconstructed surfaces. The cluster structures given are symmetrically terminated and stable and this, we believe, accounts for the low-chemical reactivity towards ammonia and methanol of clusters with these "magic numbers" of atoms.

It was also shown that a TBN Si_7 cluster can serve as the building block of the unreconstructed Si(111) surface to yield the (7×7)-reconstructed surface provided six additional TBN rest atoms are added per (7×7) unit cell.

Together, the results suggest that local-bonding concepts, as exemplified in a valence-bond context, can provide a simple useful framework for understanding the geometrical structures and electronic structures of silicon clusters. This framework allows for systematics in electronic structures among clusters to be clearly seen and for relationships between the local bonding in the bulk, at bulk surfaces, and in clusters to be identified. It promises to be a valuable theoretial supplement to the currently applied methods in unraveling the many remaining subtleties of silicon clusters.

ACKNOWLEDGMENTS

This work was supported in part by the Office of Naval Research and by the National Science Foundation MRL Program under Grant No. DMR 88 19885 at the Laboratory for Research on the Structure of Matter at the University of Pennsylvania. The authors are grateful to R. E. Smalley, M. A. Alford, M. F. Jarrold, and K. Raghavachari for helpful discussions of their respective work.

APPENDIX A: BASIS SET DETAILS

The AE basis set was the $11s7p$ basis set of Huzinaga[79(a)] contracted to $6s4p$,[79(b)] supplemented by a single-ζ ($\zeta=0.32$) d polarization basis function. The effective core potential was the shape and Hamiltonian consistent potential of Rappé *et al.*[80] This was also supplemented by a single-ζ ($\zeta=0.32$) d polarization basis function. The ECP basis set was the $2s2p$ basis set developed for the silicon effective core potential.[80] All geometry optimizations were performed using the GAMESS program[81] and single-point calculations were performed using the GVB2P5 program.[35(d),82]

APPENDIX B: COMPARISON OF METHODS

Results of geometry optimization calculations using GVB and HF wave functions and AE and ECP basis sets were given in Tables II–IV for Si_5, Si_4, and Si_3. A comparison of the binding energies for the two basis sets for all three clusters shows that the GVB-ECP binding ener-

gies are 0.01–0.02 eV/atom *less* than the GVB-AE binding energies but the HF-ECP binding energies are 0.06–0.08 eV/atom *greater* than the HF-AE binding energies. Total-energy comparisons for clusters larger than Si_5 are made at the GVB-ECP level so the results from calculations on smaller clusters indicate that their binding energies ought to be consistently slightly less than to GVB-AE binding energies (by $\sim$0.02 eV), which have not been calculated for the larger clusters. A more important point, however, is that the AE and ECP binding energies differ by a roughly constant amount, which shows that the approximations inherent in using effective core potentials do not qualitatively affect our conclusions regarding these molecules.

We also compare equilibrium bond lengths obtained with the two wave functions and basis sets. Equilibrium bond lengths for Si_5, Si_4, and Si_3 are also given in Tables II–IV. The ECP basis set yields bent-bond distances 0.00–0.01 Å longer than the AE basis set, and this is independent of the wave function used; the ECP basis set also yields long-bond distances 0.01–0.02 Å longer than the AE basis set. The GVB wave function yields bent-bond distances 0.01–0.05 Å longer than the HF wave function but the long-bond distance can be shorter (-0.07 Å in Si_4) or longer ($+0.05$ Å in Si_5) when the HF wave function is used. So the ECP basis set generally yields bond lengths slightly longer ($\sim$0.00–0.02 Å) than the AE basis set, while the GVB wave function generally yields bent bonds slightly longer ($\sim$0.01–0.05 Å) than the HF wave function but variation in the long-bond distance depends on the particular cluster. In the single case where an interstitial bond distance was optimized at both the HF and GVB-ECP levels (PBN cluster II in Table V) the HF bond distance was 2.46 Å compared to 2.51 Å, the GVB distance.

A comparison of binding energies for HF and GVB-ECP wave functions is shown in Fig. 22. Here the relative binding energies (HF or GVB) depend on the cluster size and type (PBN or TBN) because of differences in

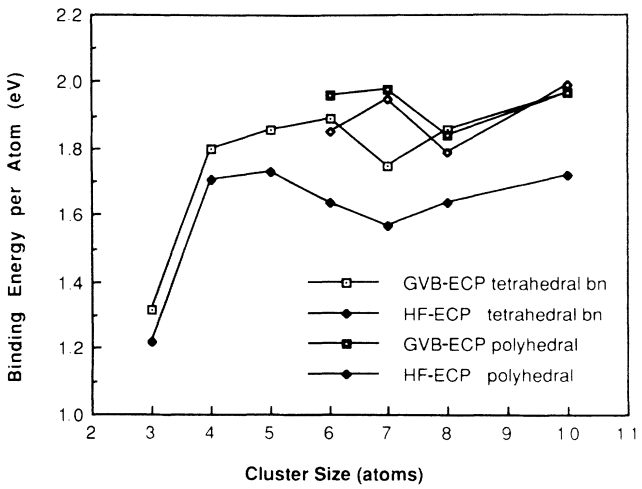

FIG. 22. Binding energies per atom calculated at the HF or GVB levels using the ECP basis set.

electronic correlation (which are included in the GVB wave function only). Note that the electron-correlation contributions to binding energy (difference in HF and GVB binding energies) are generally larger for TBN clusters, which reverses the order of stability for the Si_8 clusters and makes some TBN clusters energetically competitive with PBN clusters (D_{2d} Si_6, D_{2h} Si_{10}). [The average difference in binding energy (GVB-HF) for TBN clusters is 0.21 eV/atom with a range of 0.13–0.25 eV/atom compared to 0.04 eV/atom with a range of -0.02–0.11 eV/atom for PBN clusters. The relative *decrease* in binding energy here (-0.02 eV/atom for T_d Si_{10}) indicates that, *at the* GVB *level,* there are greater electron-correlation contributions to the total-energy per atom for the atom when compared to the cluster.] Three factors are operating here to give these differences between PBN and TBN clusters. First of all, contributions to the total energy from electron correlations are more important in TBN clusters because they have more (and longer) long bonds than PBN clusters and they have greater contributions from angular correlation of lone pairs because there are four orbitals per (lone-pair) atom in TBN clusters versus five in PBN clusters. Second, angular correlation of lone pairs or correlation of interstitial pairs in PBN clusters introduces a symmetry lowering of the GVB wave function below the nuclear symmetry: for example, in T_d Si_{10} each of the capping atoms lies on a threefold axis; the covalent-bond network to the central octahedron of atoms has this element of symmetry but an angularly correlated lone pair can only possess mirror plane and twofold rotation symmetry elements, hence the threefold rotational symmetry of those capping atoms is broken by angular correlation of the pair. A similar situation arises for the interstitial pairs when they are centered over a threefold-rotation axis, such as the interstitial pairs in T_d Si_{10} or C_{3v} Si_7. The full symmetry of the wave function could be restored by combining several VB wave functions in a RVB wave function but these would be computationally intractable because of the size of the clusters in question. However, the C_{2h} Si_8 PBN cluster gives an indication that these effects are energetically unimportant: in that cluster there are interstitial pairs and angularly correlated lone pairs but the symmetry of the cluster in such that correlating these pairs does not lower the symmetry of the wave function. In that case the contribution to the binding energy per atom from correlation is 0.04 eV/atom, which is just the average contribution. Third, TBN clusters are probably better described by the basis sets used in this work (and by other workers) than PBN clusters. All optimizations and total-energy calculations for larger clusters than Si_3 have been carried out using a double-ζ valence basis set with a single-ζ d polarization function (or in some cases other workers have used an unpolarized basis set). The polarized basis set used in this work is likely to be adequate for TBN clusters that have four localized orbitals per atom only, but calculations may be unfairly biased against PBN clusters because they have five orbitals localized on some atoms that will (relatively speaking) require a more flexible basis set in order for the five orbitals to attain their optimum shapes around the nuclei. (For example, a

second polarization function will only contribute marginally to the total energy of a ^3P Si atom but may contribute significantly to the T_d Si_{10} cluster, resulting in an *increase* in binding energy for a GVB wave function, whereas there is a net decrease in binding energy, when compared to the HF binding energy, with the current basis set.) Including a second polarization function in the basis sets of relevant clusters would present a computationally intractable problem because of basis-set size, thus the importance of this effect remains unknown.

---

*Present address: Department of Pure and Applied Physics, University of Dublin, Trinity College, Dublin 2, Ireland.

[1]O. Cheshnovsky, S. H. Yang, C. L. Pettiette, M. J. Craycraft, Y. Liu, and R. E. Smalley, Chem. Phys. Lett. **138**, 119 (1987).
[2]J. R. Heath, Y. Liu, S. C. O'Brien, Q.-L. Zhang, R. F. Curl, F. K. Tittel, and R. E. Smalley, J. Chem. Phys. **83**, 5520 (1985).
[3]M. L. Mandich, W. D. Reents, Jr., and V. E. Bondybey, J. Phys. Chem. **90**, 2315 (1986).
[4]M. L. Mandich, V. E. Bondybey, and W. D. Reents, Jr., J. Chem. Phys. **86**, 4245 (1987).
[5]J. L. Elkind, J. M. Alford, F. D. Weiss, R. T. Laaksonen, and R. E. Smalley, J. Chem. Phys. **87**, 2397 (1987).
[6]W. R. Creasey, A. O'Keefe, and J. R. McDonald, J. Phys. Chem. **91**, 2848 (1987).
[7]M. F. Jarrold, J. E. Bower, and K. Creegan, J. Chem. Phys. **90**, 3615 (1989).
[8]M. F. Jarrold and J. E. Bower, J. Phys. Chem. **92**, 5702 (1988).
[9]L. A. Bloomfield, R. R. Freeman, and W. L. Brown, Phys. Rev. Lett. **54**, 2246 (1985).
[10]Y. Liu, Q.-L. Zhang, F. K. Tittel, R. F. Curl, and R. E. Smalley, J. Chem. Phys. **85**, 7434 (1986).
[11]D. J. Trevor, D. M. Cox, K. C. Reichmann, R. O. Brickman, and A. Kaldor, J. Phys. Chem. **91**, 2598 (1987).
[12]Q.-L. Zhang, Y. Liu, R. F. Curl, F. K. Tittel, and R. E. Smalley, J. Chem. Phys. **88**, 1670 (1988).
[13]M. D. Morse, J. B. Hopkins, P. R. R. Langridge-Smith, and R. E. Smalley, J. Chem. Phys. **79**, 5316 (1983).
[14]S. M. Beck and J. M. Andrews, J. Chem. Phys. **91**, 4420 (1989).
[15]K. Raghavachari, J. Chem. Phys. **83**, 3520 (1985).
[16]K. Raghavachari and V. Logovinsky, Phys. Rev. Lett. **55**, 2853 (1985).
[17]K. Raghavachari, J. Chem. Phys. **84**, 5672 (1986).
[18]K. Raghavachari and C. M. Rohlfing, J. Chem. Phys. **89**, 2219 (1988).
[19]K. Raghavachari and C. M. Rohlfing, Chem. Phys. Lett. **143**, 428 (1988).
[20](a) D. Tomanek and M. A. Schlüter, Phys. Rev. Lett. **56**, 1055 (1986); (b) D. Tomanek and M. A. Schluter, Phys. Rev. B **36**, 1208 (1987).
[21]G. Pacchioni and J. Koutecky, J. Chem. Phys. **84**, 3301 (1986).
[22]K. Balasubramanian, Chem. Phys. Lett. **125**, 400 (1986).
[23]K. Balasubramanian, Chem. Phys. Lett. **135**, 283 (1987).
[24]P. Ballone, W. Andreoni, R. Car, and M. Parrinello, Phys. Rev. Lett. **60**, 271 (1988).
[25](a) W. N. Lipscomb, Acc. Chem. Res. **6**, 257 (1973); (b) W. N. Lipscomb, Science **196**, 1047 (1977); (c) R. W. Rudolph, Acc. Chem. Res. **9**, 446 (1976); (d) K. Wade, in *Advances in Inorganic Chemistry and Radiochemistry,* edited by H. J. Emeleus and A. G. Sharpe (Academic, New York, 1976), Vol. 18, p. 1.
[26]K. E. Khor and S. Das Sarma, Phys. Rev. B **38**, 3318 (1988); **39**, 1188 (1989).
[27]E. Blaisten-Barojas and D. Levesque, Phys. Rev. B **34**, 3910 (1986).
[28]E. Kaxiras and K. C. Pandey, Phys. Rev. B **38**, 12 736 (1988).
[29]P. A. Fedders and A. E. Carlsson, Phys. Rev. B **39**, 1134 (1989).
[30](a) J. R. Chelikowsky and R. Redwing, Solid State Commun. **64**, 843 (1987); (b) J. R. Chelikowsky, Phys. Rev. Lett. **60**, 2669 (1988); (c) J. R. Chelikowsky, J. C. Phillips, M. Kamal, and M. Strauss, *ibid.* **62**, 292 (1989); (d) J. R. Chelikowsky and J. C. Phillips, *ibid.* **63**, 1653 (1989).
[31]A. D. Mistriotis, N. Flytzanis, and S. C. Farantos, Phys. Rev. B **39**, 1212 (1989).
[32]B. C. Bolding and H. C. Andersen, Phys. Rev. B **41**, 10 568 (1990).
[33]H.-X. Wang and R. P. Messmer, Phys. Rev. B **41**, 5306 (1990).
[34]A. F. Voter and W. A. Goddard III, Chem. Phys. **57**, 253 (1982); A. F. Voter, Ph.D. thesis, California Institute of Technology, 1983 (unpublished).
[35](a) The SO and PP approximations were first suggested in A. C. Hurley, J. E. Lennard-Jones, and J. A. Pople, Proc. R. Soc. London, Ser. A **220**, 446 (1953). They were later implemented by Goddard and co-workers in their GVB wave functions. (b) P. J. Hay, W. J. Hunt, and W. A. Goddard III, J. Am. Chem. Soc. **94**, 8293 (1972); (c) W. J. Hunt, P. J. Hay, and W. A. Goddard III, J. Chem. Phys. **57**, 738 (1972); (d) F. W. Bobrowicz and W. A. Goddard III, in *Modern Theoretical Chemistry,* edited by H. F. Schaefer III (Plenum, New York, 1977), Vol. 3, Chap. 4.
[36]Overlaps of GVB orbitals in a bond pair or a lone pair usually fall into the range $\sim 0.8-0.9$; overlaps between orbitals in different pairs in carbon-carbon multiple bonds fall into the range $\sim 0.4-0.6$ [P. A. Schultz Ph.D. thesis, University of Pennsylvania, 1988 (unpublished)], which is expected to be an upper bound for overlaps between pairs forming single bonds. The large overlap of bond pairs partly accounts for the success for the Hartree-Fock wave function in most molecular situations since the spatial orbitals of that wave function are restricted to have unit overlap.
[37]L. R. Kahn, P. Baybutt, and D. G. Truhlar, J. Chem. Phys. **65**, 3826 (1976); P. J. Hay, W. R. Wadt, and L. R. Kahn, *ibid.* **68**, 3059 (1978); A. K. Rappé, T. A. Smedley, and W. A. Goddard III, J. Phys. Chem. **85**, 1662 (1981); W. R. Wadt and P. J. Hay, J. Chem. Phys. **82**, 4 (1985).
[38](a) B. Kiel, G. Stollhoff, C. Weigel, P. Fulde, and H. Stoll, Z. Phys. B **46**, 1 (1982); (b) S. Horsch, P. Horsch, and P. Fulde, Phys. Rev. B **28**, 5977 (1983); (c) **29**, 1870 (1984); (d) W. Borrmann and P. Fulde, *ibid.* **35**, 9569 (1987).
[39](a) M. D. Newton and J. M. Schulman, J. Am. Chem. Soc. **94**, 773 (1972); (b) W.-D. Stohrer and R. Hoffmann, *ibid.* **94**, 779 (1972); (c) K. B. Wiberg, *ibid.* **105**, 1227 (1983); (d) J. E. Jackson and L. C. Allen, *ibid.* **106**, 591 (1984); (e) R. P. Messmer and P. A. Schultz, *ibid.* **108**, 7407 (1986).
[40]K. B. Wiberg and F. H. Walker, J. Am. Chem. Soc. **104**, 5239 (1982).
[41]R. D. Bickerstaff and L. R. Sita, J. Am. Chem. Soc. **111**, 6454 (1989).

[42](a) G. H. F. Diercksen, N. E. Grüner, J. Oddershede, and J. R. Sabin, Chem. Phys. Lett. **117**, 29 (1985); (b) R. S. Grev and H. F. Schaefer, *ibid.* **119**, 111 (1985); R. O. Jones, Phys. Rev. A **32**, 2589 (1985).

[43]R. P. Messmer and D. R. Salahub, J. Chem. Phys. **65**, 779 (1976).

[44]G. Herzberg, in *Molecular Spectra and Molecular Structure III. Electronic Spectra and Electronic Structure of Polyatomic Molecules* (Van Nostrand, Princeton, NJ, 1966).

[45]F. A. Cotton and G. Wilkinson, in *Advances Inorganic Chemistry,* 5th Ed, (Wiley, New York, 1988), p. 457.

[46]K. C. Pandey, Phys. Rev. Lett. **47**, 1913 (1981); M. A. Olmstead, Surf. Sci. Rep. **6**, 159 (1986).

[47]M. F. Jarrold (private communication).

[48]M. A. Alford and R. E. Smalley (private communication).

[49]In Ref. 5 the minimum in reactivity is reported to occur for a cluster with 20 atoms, while neighboring peaks in reactivity were found for clusters with 18 and 23 atoms. Subsequent work, however has shown that there are *two isomers* of the 20 and 21 atom clusters and that the less reactive 21 atom cluster has the minimum reactivity (by a large factor) for all clusters with between 18 and 23 atoms [M. A. Alford and R. E. Smalley (private communication)].

[50]R. F. Curl and R. E. Smalley, Science, **242**, 1017 (1988); H. Kroto, *ibid.* **242**, 1139 (1988).

[51]R. J. Hamers, R. M. Tromp, and J. E. Demuth, Phys. Rev. B **34**, 5343 (1986).

[52]P. N. Keating, Phys. Rev. **145**, 637 (1966).

[53]H.-X. Wang and R. P. Messmer (unpublished).

[54]E. Kaxiras, Phys. Rev. Lett. **64**, 551 (1990).

[55]K. Takayanagi, Y. Tanishiro, M. Takahashi, and S. Takahashi, J. Vac. Sci. Technol. A **3**, 1502 (1985).

[56]I. K. Robinson, J. Vac. Sci. Technol. A **6**, 1966 (1988); I. K. Robinson, W. K. Waskiewicz, P. H. Fuoss, and L. J. Norton, Phys. Rev. B **37**, 4325 (1988).

[57]A. Ichimaya, Surf. Sci. **192**, L893 (1987).

[58]S. Y. Tong, H. Huang, C. M. Wei, W. E. Packard, F. K. Men, G. Glander, and M. B. Webb, J. Vac. Sci. Technol. A **6**, 615 (1988).

[59]T. Kinoshita, S. Kono, and T. Sagawa, Phys. Rev. B **34**, 3011 (1986); A. Kawazu and H. Sakama, *ibid.* **37**, 2704 (1988); G. V. Hansson, J. M. Nicholls, P. Mårtensson, and R. I. G. Uhrberg, Surf. Sic. **169**, 105 (1986); J. M. Nicholls, P. Mårtensson, G. V. Hansson, and J. E. Northrup, Phys. Rev. B **32**, 1333 (1985).

[60]S. B. DiCenzo, P. A. Bennett, D. Tribula, P. Thiry, G. K. Wertheim, and J. E. Rowe, Phys. Rev. B **31**, 2330 (1985); J. S. Pedersen, R. Feidenhans'l, M. Nielsen, F. Grey, and R. L. Johnson, *ibid.* **38**, 13 210 (1988).

[61]R. I. G. Uhrberg, R. D. Bringans, M. A. Olmstead, R. Z. Bachrach, and J. E. Northrup, Phys. Rev. B **35**, 3945 (1987); R. S. Becker, B. S. Schwartzenruber, M. S. Hybertsen, and S. G. Louie, Phys. Rev. Lett. **60**, 116 (1988); R. L. Headrick, and W. R. Graham, Phys. Rev. B **37**, 1051 (1988); J. R. Patel, J. A. Golovchenko, P. E. Freeland, and H.-J. Gossmann, *ibid.* **36**, 7715 (1987); M. Copel, R. M. Tromp, and U. K. Kohler, *ibid.* **37**, 10 756 (1988); R. D. Bringans, R. I. G. Uhrberg, R. Z. Bachrach, and J. E. Northrup, Phys. Rev. Lett. **55**, 533 (1985).

[62]R. S. Becker, B. S. Schwartzenruber, and J. S. Vickers, J. Vac. Sci. Technol. A **6**, 472 (1988); R. S. Becker, B. S. Schwartzenruber, J. S. Vickers, and T. Klitsner, Phys. Rev. B **39**, 1633 (1989).

[63]H. J. Gossman, J. C. Bean, L. C. Feldman, E. G. McRae, and I. K. Robinson, Phys. Rev. Lett. **55**, 1106 (1985).

[64]J. Aarts, A. J. Hoeven, and P. K. Larsen, Phys. Rev. B **37**, 8190 (1988); P. M. J. Marée, K, Nakagawa, J. F. van der Veen, and R. M. Tromp, Phys. Rev. B **38**, 1585 (1988).

[65]D. Vanderbilt, Phys. Rev. Lett. **59**, 1456 (1987); R. D. Meade and D. Vanderbilt, Phys. Rev. Lett. **63**, 1404 (1989).

[66]G.-X. Qian, and D. J. Chadi, J. Vac. Sci. Technol. B **4**, 1079 (1986); G.-X. Qian, and D. J. Chadi, Phys. Rev. B **35**, 1288 (1987).

[67]H. Olijnyk, S. K. Sikka, and W. B. Holzapfel, Phys. Lett. **103A**, 137 (1984).

[68]J. Z. Hu and I. L. Spain, Solid State Commun. **51**, 263 (1984).

[69]K. J. Chang, M. M. Dacorogna, M. L. Cohen, J. M. Mignot, G. Chouteau, and G. Martinez, Phys. Rev. Lett. **54**, 2375 (1985).

[70]T. H. Lin, W. Y. Dong, K. J. Dunn, C. N. J. Wagner, and F. P. Bundy, Phys. Rev. B **33**, 7820 (1986).

[71]D. Erskine, P. Y. Yu, K. J. Chang, and M. L. Cohen, Phys. Rev. Lett. **57**, 2741 (1986).

[72]S. J. Duclos, Y. K. Vohra, and A. L. Ruhoff, Phys. Rev. Lett. **58**, 775 (1987).

[73]M. T. Yin and M. L. Cohen, Phys. Rev. B **26**, 566 (1982).

[74]M. T. Yin, Phys. Rev. B **30**, 1773 (1984).

[75]K. J. Chang and M. L. Cohen, Phys. Rev. B **31**, 7819 (1985).

[76]J. R. Chelikowsky, Phys. Rev. B **35**, 1174 (1987).

[77]A. Y. Liu, K. J. Chang, and M. L. Cohen, Phys. Rev. B **37**, 6344 (1988).

[78]Y. Kuk, M. F. Jarrold, P. J. Silverman, J. E. Bower, and W. L. Brown, Phys. Rev. B **39**, 11 168 (1980).

[79](a) S. Huzinaga, Department of Chemistry, The University of Alberta, Canada report 1971 (unpublished); (b) T. H. Dunning, Jr. and P. J. Hay, in *Modern Theoretical Chemistry* (Plenum, New York, 1977), Vol. 4, p. 1.

[80]A. K. Rappé, T. A. Smedley, and W. A. Goddard III, J. Phys. Chem. **85**, 1662 (1981).

[81]M. Dupuis, D. Spangler, J. Wendoloski, S. Elbert, M. Schmidt, GAMESS program Version 1.02, Revision 10 (1987), National Resource for Computation in Chemistry Software Catalog Vol. 1, Program QG01 (1980), Lawrence Berkeley Laboratory, United States Department of Energy.

[82](a) R. A. Bair, W. A. Goddard III, A. F. Voter, A. K. Rappé, L. G. Yaffe, F. W. Bobrowicz, W. R. Wadt, P. J. Hay, and W. J. Hunt, GVB2P5 program (unpublished); (b) P. J. Hay, W. J. Hunt, and W. A. Goddard III, J. Am. Chem. Soc. **94**, 8293 (1972); (c) W. J. Hunt, P. J. Hay, and W. A. Goddard III, J. Chem. Phys. **57**, 738 (1972).

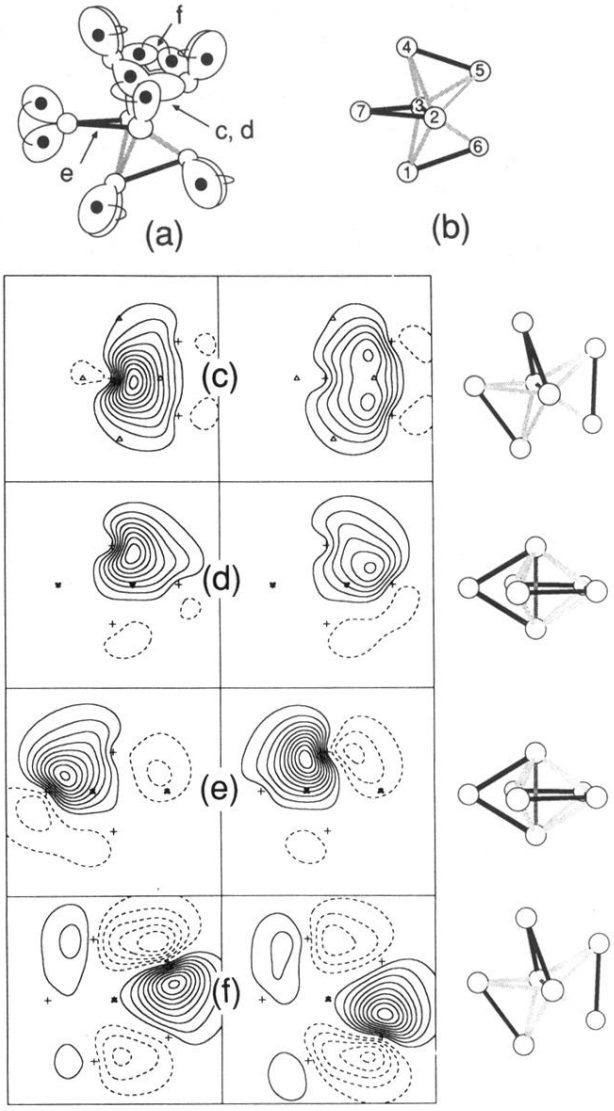

FIG. 11. (a) Schematic diagram and (b) molecular structure of PBN D_{5h} $^1A_1'$ Si_7; (c) orbitals forming the Si(2)-Si(4)-Si(5) interstitial pair; (d) the same interstitial pair orbitals in a plane containing Si(2), Si(3), and Si(6); (e) orbitals forming the Si(2)—Si(7) bent-bond pair; (f) orbitals forming the Si(4)—Si(5) bond pair.

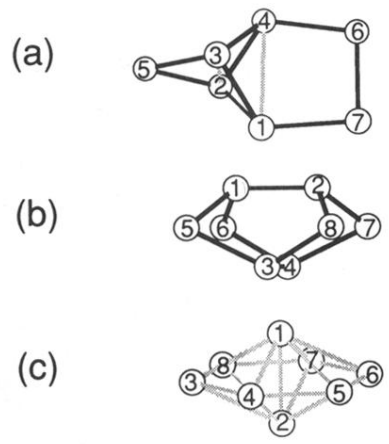

FIG. 12. Molecular structures for (a) TBN C_{2v} Si_7; (b) TBN D_{2d} Si_8; (c) PBN D_{6h} Si_8.

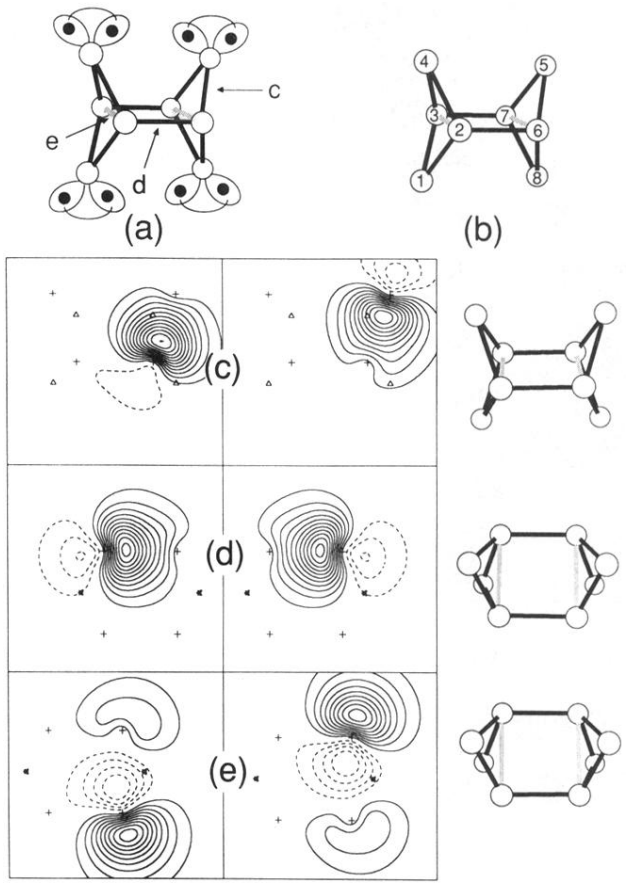

FIG. 13. (a) Schematic diagram and (b) molecular structure of ^1A_g D_{2h} TBN Si_8; (c) orbitals forming the Si(5)—Si(6) bent bond; (d) orbitals forming the Si(2)—Si(6) bent bond; (e) orbitals forming the Si(6)—Si(7) long bond.

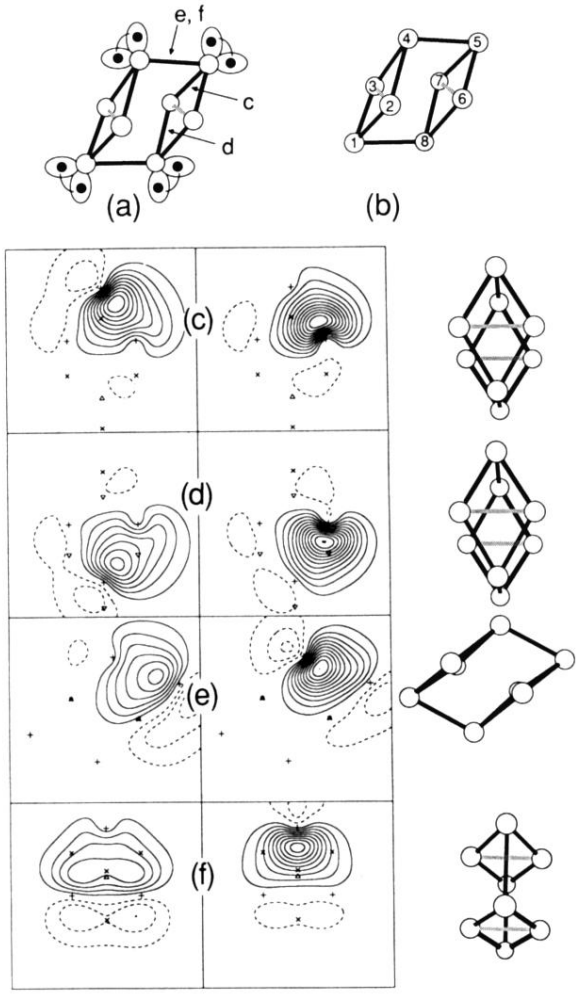

FIG. 14. (a) Schematic diagram and (b) molecular structure of PBN C_{2h} ^1A_g Si_8; (c) orbitals forming the Si(5)—Si(7) bent bond; (d) orbitals forming the Si(7)—Si(8) bent bond; (e) orbitals forming the Si(4)-Si(5)-Si(6)-Si(7) interstitial pair; (f) the same pair in a plane containing atoms Si(4), Si(6), and Si(7) showing the interstitial δ character of the pair.

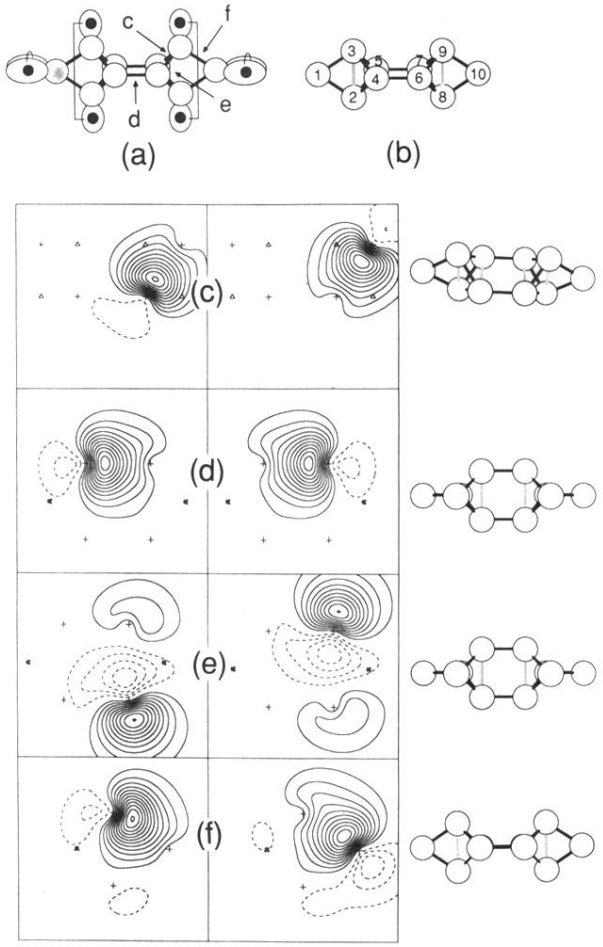

FIG. 15. (a) Schematic diagram and (b) molecular structure of TBN D_{2h} ^1A_g Si_{10}; (c) orbitals forming the Si(6)—Si(9) bent bond; (d) orbitals forming the Si(5)—Si(7) bent bond; (e) orbitals forming the Si(6)—Si(7) long bond; (f) orbitals forming the Si(9)—Si(10) bent bond.

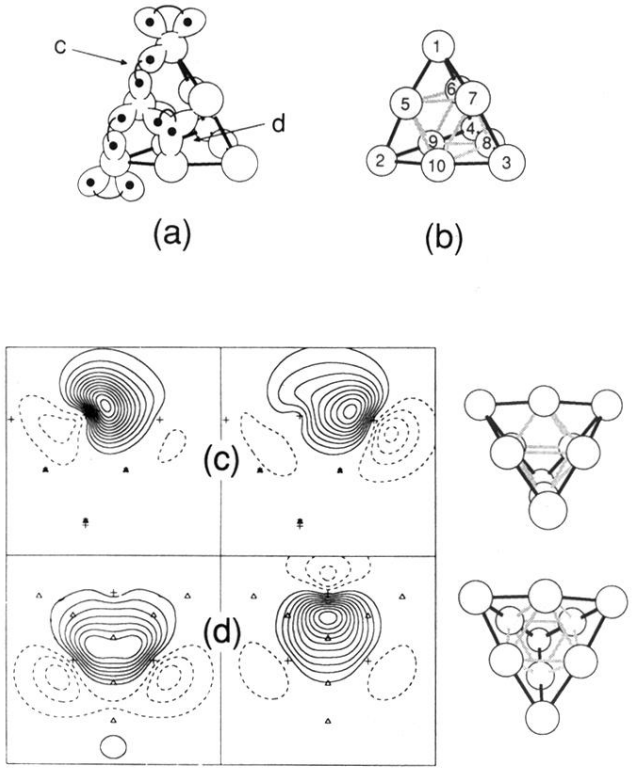

FIG. 16. (a) Schematic diagram and (b) molecular structure of PBN T_d $^1A_1$ Si_{10}; (c) orbitals forming the Si(1)—Si(5) bent-bond pair; (d) orbitals forming the Si(5)-Si(7)-Si(10) interstitial pair.

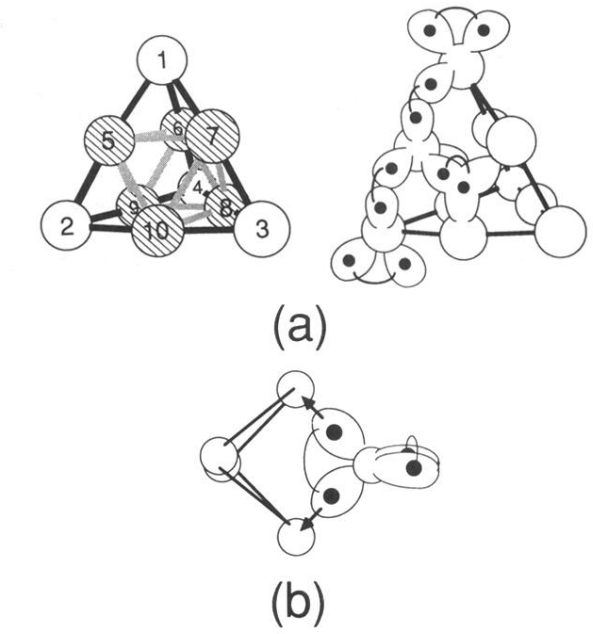

FIG. 2. (a) Geometrical structure and schematic GVB orbital diagrams for T_d Si_{10}. In the structure diagram on the left the central octahedron of atoms is outlined by shaded lines, while the tetrahedral capping atoms are joined to it by solid lines. At the top of the diagram on the right, a capping atom (atom 1 at left) is shown with an angularly correlated lone pair and three bonds to octahedral atoms (one is shown with singlet paired orbitals and the other two are shown with solid lines). In the right diagram the schematic orbitals on one atom (atom 5 at left) of the central octahedron are shown explicitly; those atoms have four tetrahedral orbitals, two are used to form bonds to capping atoms and two form parts of interstitial pairs in different faces of the cluster. An interstitial bond pair (in the triangular face formed by atoms 5, 7, and 10 in the left diagram) is shown at the right. These are all the unique electron pairs in the cluster. (b) Schematic representation of three-center dative bonds.

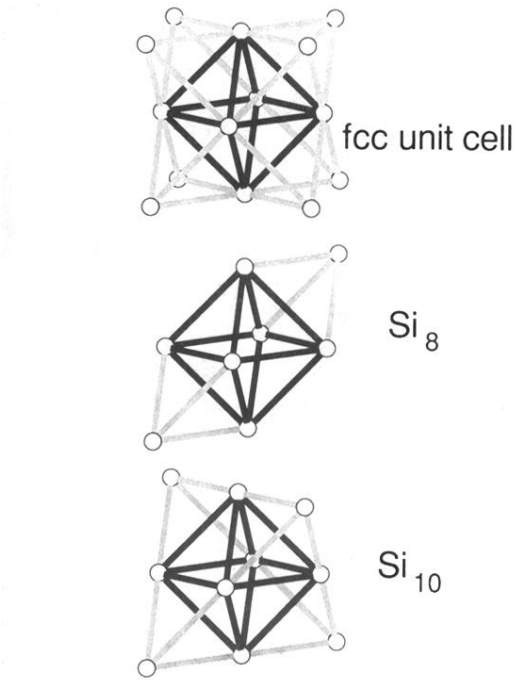

FIG. 20. A comparison of structures of an fcc cell and PBN Si_8 and Si_{10} clusters. The octahedral interstitial site enclosed in the unit cell is outlined by solid lines and the tetrahedral sites are outlined by shaded lines.

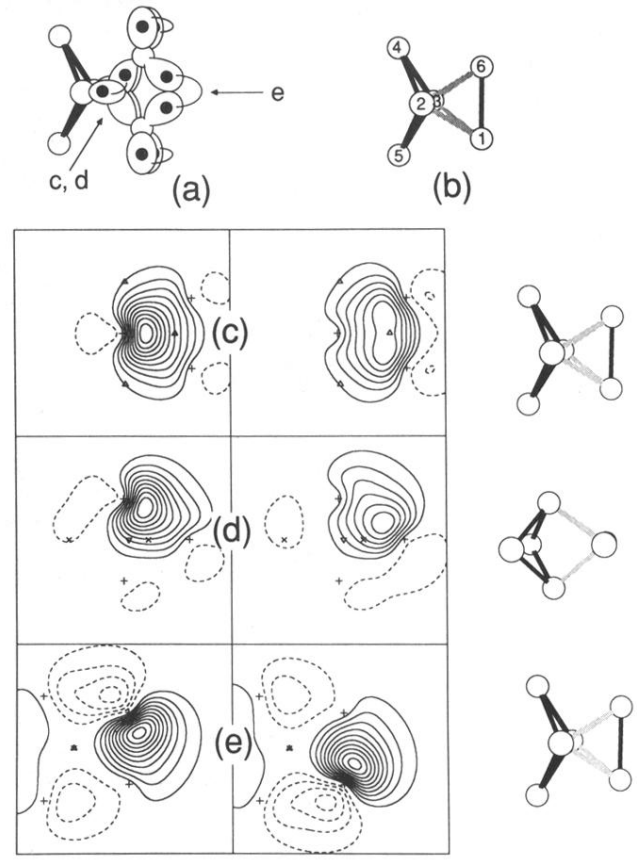

FIG. 9. (a) Schematic diagram and (b) molecular structure of PBN C_{2v} $^1A_1$ Si_6; (c) orbitals forming the Si(2)—Si(1)—Si(6) interstitial pair; (d) the same interstitial pair orbitals in a plane containing Si(2), Si(1), and Si(3); (e) orbitals forming the Si(1)—Si(6) bond.